NIST Technical Note
NIST TN 2382

Evaluation and Modification of Commercial Equipment to Evaluate Air Permeability of Concrete

Stephanie S. Watson
Ashley S. Carey
Benjamin Johnsson

This publication is available free of charge from:
https://doi.org/10.6028/NIST.TN.2382

NIST NATIONAL INSTITUTE OF STANDARDS AND TECHNOLOGY
U.S. DEPARTMENT OF COMMERCE

NIST Technical Note
NIST TN 2382

Evaluation and Modification of Commercial Equipment to Evaluate Air Permeability of Concrete

Stephanie S. Watsonł
Material and Structural Systems Division
Engineering Laboratory

Ashley S. Carey*ł
Benjamin Johnsson*

**Former NIST employee; all work for this publication was done while at NIST*
ł Authors contributed equally to this report

This publication is available free of charge from:
https://doi.org/10.6028/NIST.TN.2382

September 2026

U.S. Department of Commerce
Howard Lutnick, Secretary

National Institute of Standards and Technology
Arvind Raman, NIST Director and Under Secretary of Commerce for Standards and Technology

NIST TN 2382
September 2026

Publication History
Approved by the NIST Editorial Review Board on 2026-09-15

How to Cite this NIST Technical Series Publication
Watson SS, Carey AS, and Johnsson B (Year) Evaluation and Modification of Commercial Equipment to Evaluate Air Permeability of Concrete. (National Institute of Standards and Technology, Gaithersburg, MD), NIST Technical Note (TN) NIST TN 2382. https://doi.org/10.6028/NIST.TN.2382

Author ORCID iDs
Stephanie S. Watson: 0009-0003-2001-5592
Ashley S. Carey: 0000-0002-8741-258X
Benjamin Johnsson: 0009-0008-8513-0483

Contact Information
Stephanie S Watson, Ph.D.
stephanie.watson@nist.gov

Abstract

Pyrrhotite in concrete aggregate can lead to severe cracking due to expansion reactions. Most research has focused on screening methods and mix designs that lower the permeability of new structures. However, there is a need to evaluate the feasibility of mitigation techniques for existing structures containing pyrrhotite aggregate but have not yet shown signs of deterioration. Efforts at NIST have focused on evaluating the potential of concrete sealants, which can reduce or entirely eliminate the ingress of water and air into the concrete. Since pyrrhotite requires both oxygen and water to react, one or both component's concentrations can be reduced to delay pyrrhotite oxidation for some amount of time. One methodology being vetted for characterizing the performance of mitigating sealants is air permeability test. This report details efforts to validate changes made to a commercially available air permeameter to better facilitate NIST's needs. This validation testing was generally conducted in two parts. Part 1 focused on validating as-received equipment for use with 152.4 mm (6-inch) diameter concrete cores, which is the size the commercially available set-up is made to test. Part 2 focused on validating retrofitting the equipment to test 101.6 mm (4-inch) diameter cores, the common diameter used for laboratory and field-cast concrete specimens.

Keywords

Air Permeability; Concrete; Pyrrhotite; RILEM-Cembureau Permeability

Table of Contents

1. Introduction and Background 1
1.1. Pyrrhotite Damage in Concrete Structures 1
1.2. Overview of Pyrrhotite Oxidation Mechanisms 3
1.3. Objectives and Scope 4
2. Overview of Air Permeability – Theory and Equipment 6
2.1. Constant Pressure Theory for Air Permeability 6
2.2. RILEM-Cembureau Methodology 7
2.3. Experimental Set-Up and Standard Operating Procedure Used at NIST 7
3. Validation of Air Permeability Equipment for 152.4 mm (6-inch) Diameter Specimens 12
3.1. Materials and Specimen Preparation 12
3.2. Results 13
3.2.1. Objective 1; Experiment A – Flow Rate Measurement Method 13
3.2.2. Objective 1; Experiment B – Minimum Rubber Tube Inflation Pressure 15
3.2.3. Objective 1; Experiment C – Preconditioning Protocols 17
3.2.4. Objective 2; Experiment A – Repeatability of Testing Protocol 19
3.2.5. Objective 2; Experiment B – w/cm Ratio Trends 20
3.2.6. Objective 2; Experiment C – Sensitivity of Equipment to Sealants 21
4. Validation of Air Permeability Equipment for 101.6 mm (4-inch) Diameter Specimens 23
4.1. Materials and Specimen Preparation 23
4.2. Results 25
4.2.1. Objective 1 – Validation of Modified Testing Set-Up for 101.6 mm Diameter Specimens 25
4.2.2. Objective 2 – Accuracy of Air Permeability Measurements for Specimens with Heights Less Than 50 mm 29
5. Summary and Conclusions 32
5.1. Findings from Goal 1 – Validating Equipment to Test 152.4 mm Diameter Specimens 32
5.2. Findings from Goal 2 – Retrofitting Equipment to Test 101.6 mm Diameter Specimens 32
References 34
Appendix A. List of Symbols, Abbreviations, and Acronyms 36
A.1. Symbols 36
A.2. Acronyms/Abbreviations 37
A.3. General Chemistry Notation 37
A.4. Cement Chemistry Notation 37

List of Tables

Table 1. Volumetric Expansion of Pyrrhotite-Related Reactions.....3
Table 2. Summary of Goal 1 objectives and corresponding experiments 12
Table 3. Concrete materials and mix design used for validation of 152.4 mm (6-inch) diameter cores.12
Table 4 Concrete materials and mix design used for validation of 101.6 mm (4-inch) diameter cores..23
Table 5. Measured heights of Goal 2 specimens after initial sawing.....25
Table 6. Summary of statistical analysis of w/cm ratio on permeability for each specimen size 28
Table 7. Measured heights of 101.6 mm diameter specimens after trimming.....30

List of Figures

Figure 1. Photographs of deteriorated foundations sampled by NIST personnel in April and August 2024 detailing the level of damage typically seen in foundations prior to replacement and removal **2**

Figure 2. Overview of pyrrhotite oxidation process and associated damage mechanisms **4**

Figure 3. Overview testing and associated objectives with each goal **5**

Figure 4. Schematic of the RILEM-Cembureau air permeability test equipment: (a) overall view; (b) detailed schematic of permeameter cell **7**

Figure 5. As-received RILEM-Cembureau permeability equipment manufactured by Controls Group **8**

Figure 6. Placing concrete specimen into permeameter cell **9**

Figure 7. Rubber tube inflation: (a) 965 kPa capacity air compressor; (b) valve stem extender; (c) inflation gun with gauge **10**

Figure 8. Schematic of rubber inserts designed for testing of 4-inch diameter concrete specimens in air permeability cell **11**

Figure 9. Machined neoprene inserts: (a) side view of two machined inserts; (b) two inserts stacked for testing **11**

Figure 10. Mixing and specimen preparation: (a) fresh concrete in 0.02 m^2 bucket mixer; (b) cast 15.2 cm by 30.5 cm specimens of varying w/cm ratios; (c) cutting specimens with masonry block saw; (d) sealed and unsealed pucks ready for testing **13**

Figure 11. Comparison of apparent permeability calculated using soap bubble and digital flow meters **14**

Figure 12. Theoretical relationship between rubber tube pressure and apparent permeability **15**

Figure 13. Influence of rubber tube pressure on measured air permeability **17**

Figure 14. Comparison of preconditioning methods for air permeability measurements **19**

Figure 15. Repeatability of air permeability measurements on a single specimen **20**

Figure 16. Measured apparent permeability as a function of concrete w/cm ratio **21**

Figure 17. Measured apparent permeability for sealed concrete specimens **22**

Figure 18. Mixing and curing process used for specimens to meet Goal 2 of study: (a) mixing concrete in bucket mixer; (b) initial 24 hour curing in sealed containers in temperature-controlled chamber; (c) room temperature, 100 % relative humidity curing chamber **24**

Figure 19. Manufactured neoprene rings: (a) view with 101.6 mm concrete specimen inserted; (b) 101.6 mm concrete specimen with neoprene rings in concrete air permeability cell **26**

Figure 20. Comparison of measured air permeability for 152.4 mm and 101.6 mm specimens tested in the RILEM-Cembureau air permeability set-up **27**

Figure 21. Comparison of air permeability trends for 152.4 mm and 101.6 mm diameter specimens **29**

Figure 22. Comparison of measured air permeability for 101.6 mm specimens with varying heights tested in the RILEM-Cembureau air permeability set-up **31**

NIST Disclaimer

Identifying any commercial product or trade name does not imply endorsement or recommendation by NIST. The policy of NIST is to use metric units of measurement in all its publications and to provide statements of uncertainty for all original measurements. In this document, however, data from organizations outside NIST are shown, which may include measurements in non-metric units or measurements without uncertainty. Unless otherwise specified, the uncertainties shown are equal to +/- one standard deviation.

Acknowledgments

This research was conducted to support the congressionally funded STRS project “Assessing Pyrrhotite in Concrete”. The authors are also grateful for the financial support of the Summer Undergraduate Research Fellowship (SURF) program, which funded Benjamin Johnsson’s research at NIST.

1. Introduction and Background

1.1. Pyrrhotite Damage in Concrete Structures

Concrete foundations in Connecticut and Massachusetts are crumbling due to the inclusion of the iron-sulfide mineral pyrrhotite in aggregates used in the concrete. Affected foundations were constructed between the 1980s and 2010s, and over this long time span, pyrrhotite began to oxidize as it was exposed to water and oxygen leading to extreme cracking and loss of structural integrity of the foundation walls (Figure 1). It is estimated that 5,000 foundations in Connecticut were built using pyrrhotite-bearing aggregate; however, the Connecticut Department of Housing estimates that upwards of 35,000 foundations could have been built with pyrrhotite-bearing aggregate [1,2]. In many cases, homeowners are unaware of the ongoing pyrrhotite oxidation until cracking begins to show on foundation walls. At that point, it is often too late to employ mitigation strategies to prolong the lifespan of the foundation, and homeowners are left with no choice but to remove and replace it.

State governments in both Connecticut and Massachusetts have passed legislation outlining maximum sulfur content thresholds for all aggregates used in concrete mixtures and mandating that all quarries that sell aggregate for concrete must test their aggregate regularly to ensure the sulfur content is below the mandated threshold [3,4]. In both states, a total sulfur content less than 0.1 % means an aggregate is clean and can be used in concrete. A total sulfur content of (0.1 to 1.0) % requires additional testing to determine which sulfide minerals are present in the aggregate (e.g., pyrrhotite, pyrite, chalcopyrite, etc.). If a quarry reports a total sulfur content greater than 1.0 % then the aggregate cannot be used in concrete mixtures. However, there is no widely accepted testing protocol to determine the total sulfur content of aggregates, which has led to uncertainty in the effectiveness of the state legislation [5]. To fill this gap, many research efforts have evaluated various methods to consistently screen aggregate for pyrrhotite oxidation potential such as multi-step aggregate screening frameworks [8, 9], oxidation testing protocols [6,7], and thermomagnetic testing protocols [10, 11]. The potential of these frameworks and testing protocols to identify pyrrhotite-bearing aggregate is high; however, more research is needed to refine these protocols and ultimately acceptance/rejection criteria for aggregate sources, as these criteria have considerable economic implications on concrete aggregate production and supply.

Figure 1. Photographs of deteriorated foundations sampled by NIST personnel in April and August 2024 detailing the level of damage typically seen in foundations prior to replacement and removal

1.2. Overview of Pyrrhotite Oxidation Mechanisms

Pyrrhotite ($Fe_{1-x}S$, $0 \leq x \leq 0.125$) is an iron-sulfide mineral with variable iron content that is naturally occurring in all rock types [12]. Compared to other types of iron sulfide minerals such as pyrite, pyrrhotite is very reactive when exposed to oxygen and water [13]. When used in a concrete mixture, deterioration of the structure due to pyrrhotite oxidation typically occurs in three phases (Figure 2). In Phase 1, oxygen and water infiltrate through the concrete matrix to reach aggregates with pyrrhotite and oxidation is started. In Phase 2, as pyrrhotite oxidation continues, iron byproducts such as ferrihydrite, $Fe_{10}O_{14}(OH)_2$, and goethite, FeO(OH), form and cause the surrounding aggregate to crack due to the associated increase in volume. Ferrihydrite is a complex mineral and is not fully characterized; as a result, it has been oversimplified in cases and reported as $Fe(OH)_3$ which is not entirely accurate [14]. As the aggregate cracks, sulfates (SO_4^{2-}) that are generated during pyrrhotite oxidation are mobilized and can move into the surrounding cement paste matrix. As seen in Figure 2, Phase 2, the pyrrhotite generally oxidizes and releases sulfates in bands. The gray bands are regions of the pyrrhotite where the sulfur is no longer present, while the yellow sections contain sulfur. During Phase 3, leached sulfates begin to react with alumina-rich phases of the cement paste matrix such as unhydrated calcium aluminate (C_3A) and calcium aluminate monosulfate hydrate ($C_4A\overline{S}H_{12}$). Internal sulfate attack leads to the precipitation of volumetrically larger minerals such as gypsum ($C\overline{S}H_2$), ettringite ($C_6A\overline{S}_3H_{32}$), and thaumasite ($C_3S\overline{C}\text{-}\overline{S}\text{-}H_{15}$) which leads to additional cracking of the cementitious matrix. Table 1 illustrates the range in volume change for all pyrrhotite related reactions. Figure 2, Phase 3 shows a scanning electron microscope (SEM) image of ettringite (colored in yellow due to its sulfur content) that has precipitated in an existing air void.

Table 1. Volumetric Expansion of Pyrrhotite-Related Reactions

	Chemical Formula	**Volume Change (cm^3/mole sulfide) [15]**
Ferrihydrite	$Fe(OH)_3$	6.14
Geothite	FeO(OH)	0.64
Gypsum	$C\overline{S}H_2$	41.6
Calcium Monosulfoaluminate	$C_4A\overline{S}H_{12}$	182.9
Ettringite	$C_6A\overline{S}_3H_{32}$	172.2
Thaumasite	$C_3S\overline{C}\text{-}\overline{S}\text{-}H_{15}$	141.2

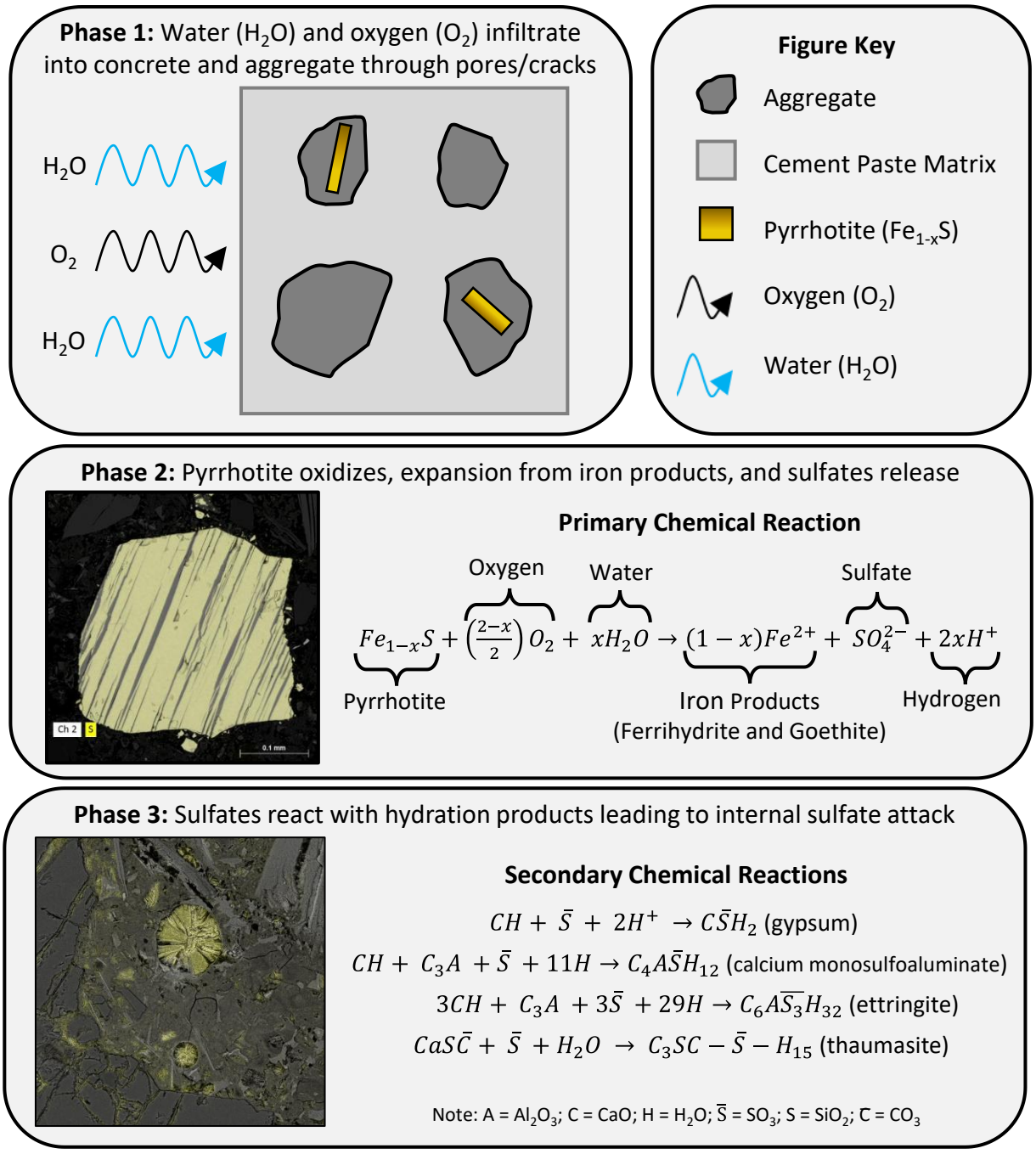

Figure 2. Overview of pyrrhotite oxidation process and associated damage mechanisms

1.3. Objectives and Scope

Research regarding pyrrhotite in concrete aggregate has primarily focused on screening frameworks and altering concrete mix designs that reduce the permeability of new structures; however, there is a need to evaluate the feasibility of mitigation techniques for existing structures that were built with pyrrhotite aggregate but have yet to show signs of deterioration [16]. Efforts at NIST have focused on evaluating the potential of concrete sealants, which can

reduce or altogether stop the flow of water and/or air into the concrete. Since pyrrhotite needs both oxygen and water to oxidize, if one or both components' concentrations can be decreased, then pyrrhotite oxidation can be delayed for some amount of time. While there are claims from the concrete community that trapped water and oxygen already contained within the existing concrete could fuel the chemical reaction, measurement evidence for sealants not reducing damage is lacking. Furthermore, in the field NIST observed less damage, by way of lower concentrations of foundation cracks and better mechanical properties measured in core specimens, for a 'younger' house on which a substantial membrane type sealant was applied to the exterior only. It should be noted that the goal of NIST's research is to establish measurement tools to confirm the efficacy of sealants applied to concrete materials.

One methodology being vetted for characterizing the performance of varying mitigating sealants is air permeability test. This report details efforts taken by the authors to validate changes made to a commercially available air permeameter to better facilitate NIST's testing needs. This testing generally occurred with two goals as detailed in Figure 3. Goal 1 was focused on validating as-received equipment for use with 152.4 mm (6-inch) diameter concrete cores, which is the size the commercially available set-up is made to test. Goal 2 was focused on validating retrofits to the equipment to allow for the testing of 101.6 mm (4-inch) diameter cores, which is the common diameter used in laboratory and field cast concrete specimens.

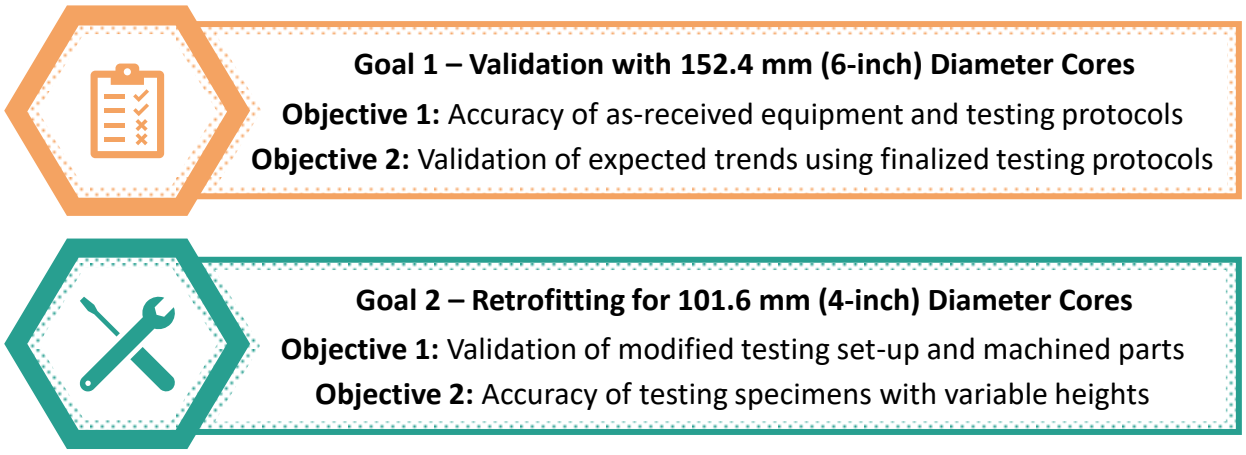

Figure 3. Overview testing and associated objectives with each goal

2. Overview of Air Permeability – Theory and Equipment

Air permeability is a common metric used when assessing transport properties of concrete materials. However, there is not a specific standardized methodology that is universally accepted. Several methods are used throughout the concrete materials testing community, but all these methods are founded on the theoretical basis of constant pressure or variable pressure tests. This report reviews the constant pressure theory and the RILEM-Cembureau methodology, as these are the experimental set-up utilized.

2.1. Constant Pressure Theory for Air Permeability

For an air permeability test to fall under the constant pressure theory, one surface of the test specimen must be exposed to constant pressure for the duration of the test, while air flow through the opposite surface of the specimen is measured until a constant flow rate is reached. To calculate apparent air permeability (k_A), a modified version of Darcy's Law is used as shown in Equation 1. Once apparent permeability is calculated, intrinsic permeability (k_0) can be determined by applying the Klinkenberg correction factor (b) to account for the boundary condition and potential gas slippage, which can cause overestimation of permeability (Equation 2) [17, 18]. The gas slippage effect is a phenomenon where the mean free path of gas molecules has comparable magnitude to the pore diameter such that a gas molecule will not collide with other molecules, resulting in a faster gas flow rate through the pore. This slippage effect is only applicable to a capillary with negligible length and uniform diameter distribution.

$$k_A = \frac{2Qp_aL\mu}{A(p^2 - p_a^2)} \quad \text{(Eq. 1)}$$

$$k_A = k_0\left(1 + \frac{2b}{p + p_a}\right) \quad \text{(Eq. 2)}$$

Where:

k_A is apparent gas permeability [m^2]

Q is volumetric flow rate of the gas [m^3/s]

p_a is outlet pressure/atmospheric pressure [Pa]

L is thickness of the specimens in the direction of gas flow [m]

μ is dynamic viscosity of the gas at test temperature [$N{\cdot}s/m^2$]

A is cross-sectional area of the specimen [m^2]

p is inlet pressure [Pa]

k_0 is intrinsic gas permeability [m^2]

b is the Klinkenberg correction factor [Pa]

2.2. RILEM-Cembureau Methodology

Development of the RILEM-Cembureau method to measure air permeability was initiated in the 1980s by a committee formed from members Cembureau, the European Cement Association. This committee, denoted as TC 116, had two primary objectives: 1) develop a method for the measurement of permeability of concrete for a gas or water, and 2) establish the feasibility of obtaining consistent results in several laboratories [19]. In 1999, the International Union of Laboratories and Experts in Construction Materials, Systems, and Structures (RILEM) published a draft standard for air permeability outlining the experimental method [20] as well as a final report detailing the results of an interlaboratory study [21]. One recommendation developed as a result of the interlaboratory study was the implementation of a preconditioning protocol as there was a strong relationship between specimen moisture content and measured permeability.

The RILEM-Cembureau method uses specimens with a 152.4 mm (6-inch) diameter and a thickness of 50.8 mm (2-inches). During testing, specimens are laterally confined using a rubber ring and an inflated tube to promote one-dimensional gas flow with little to no slippage around the specimen. At a minimum, three gas inlet pressures should be used to develop an average air permeability; however, in many cases five inlet pressures are used when measuring permeability. Equipment needed to conduct RILEM-Cembureau permeability tests is commercially available, and a schematic of the equipment is shown in Figure 4.

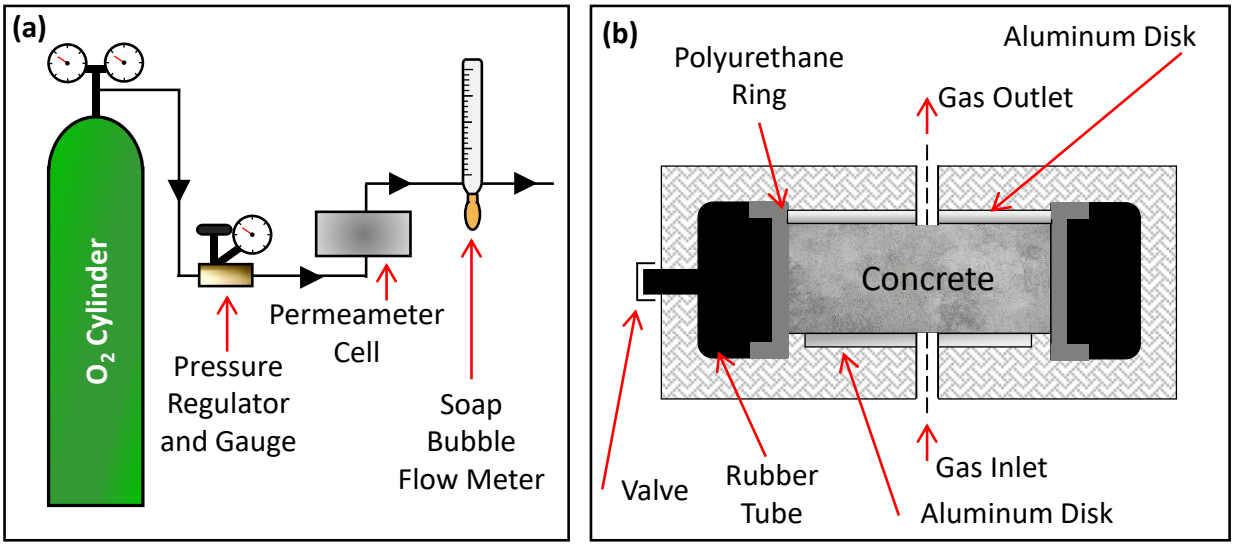

Figure 4. Schematic of the RILEM-Cembureau air permeability test equipment: (a) overall view; (b) detailed schematic of permeameter cell

2.3. Experimental Set-Up and Standard Operating Procedure Used at NIST

A RILEM-Cembureau permeability set-up was purchased by the Infrastructure Materials Group in early 2024 from Controls Group (Liscate, Lombardia, Italy). Figure 5 shows photographs of the as-received equipment system in the lab. All equipment and tubing were provided by Controls Group with the exception of the gas cylinder and regulator as well as the frame used to

hold the provided metal panel. A 6,230-liter (220 cubic foot) capacity oxygen cylinder with a purity of 99.5 % and oxygen-specific regulator was obtained for all testing with the permeability equipment as the length of the test requires this size of tank. The manufacturer supplied equipment included a pressure regulator rated for up to 1034 kPa (150 psi) and a pressure gauge rated for up to 500 kPa (72.5 psi). Additionally, three soap bubble flow meters with volumes of 10 mL, 25 mL, and 100 mL, respectively, were included to ensure concrete with a range of air permeabilities could be adequately measured. In addition to the soap bubble flow meters, an Omega FMA-1600A digital volumetric flow meter with a maximum flow rate of 2 standard liters per minute was used to measure the quantity of oxygen that permeated through a concrete specimen in this study.

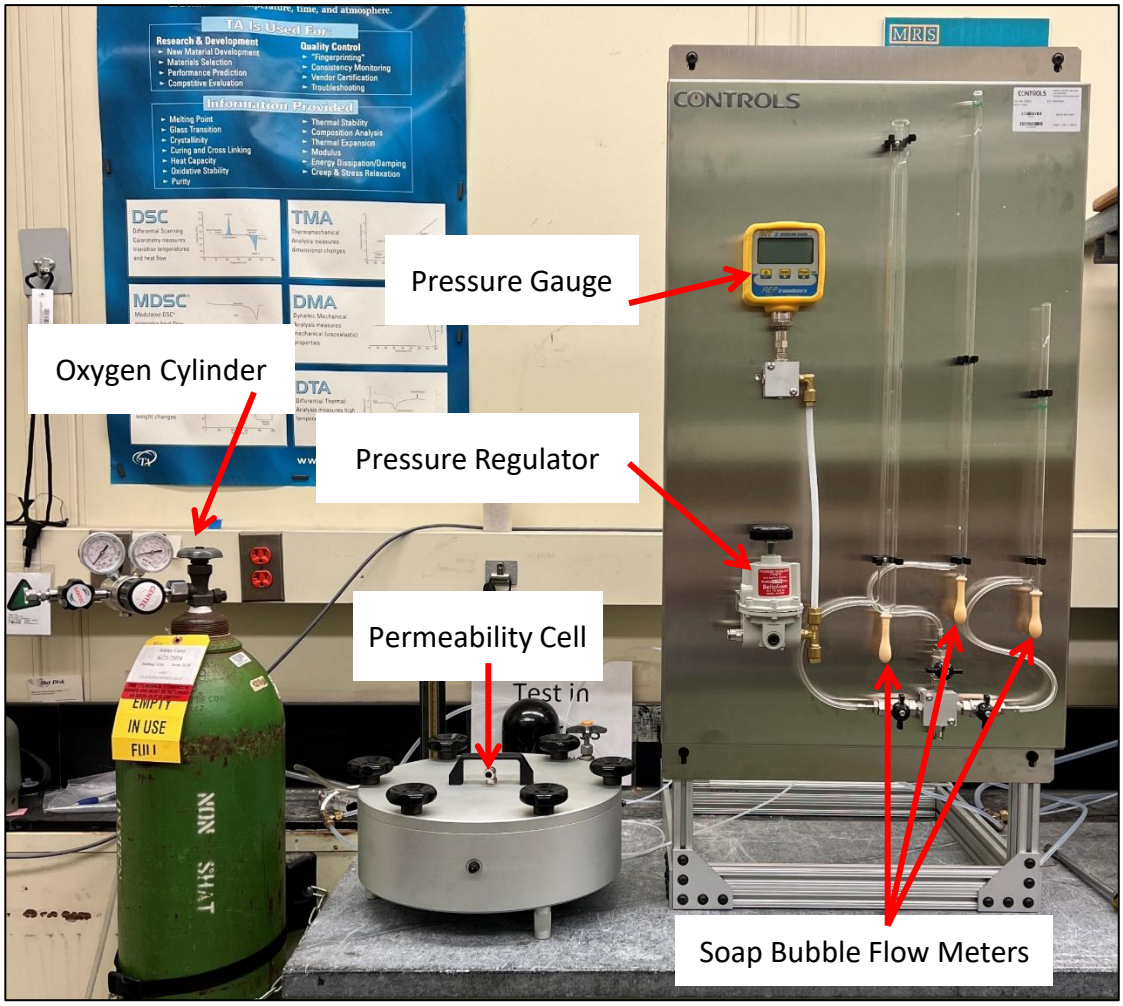

Figure 5. As-received RILEM-Cembureau permeability equipment manufactured by Controls Group

Based on the manufacturer's operation manual, a standard operating procedure was developed to ensure safe usage of the equipment. When testing a concrete specimen, it was inserted into the rubber sleeve of the permeameter cell (Figure 6a; Figure 6b), and then an aluminum disc was placed on top of the specimen with the inscribed face facing the specimen (Figure 6c). The permeameter lid was then placed on top of the cell and screwed into place using the provided hand screws.

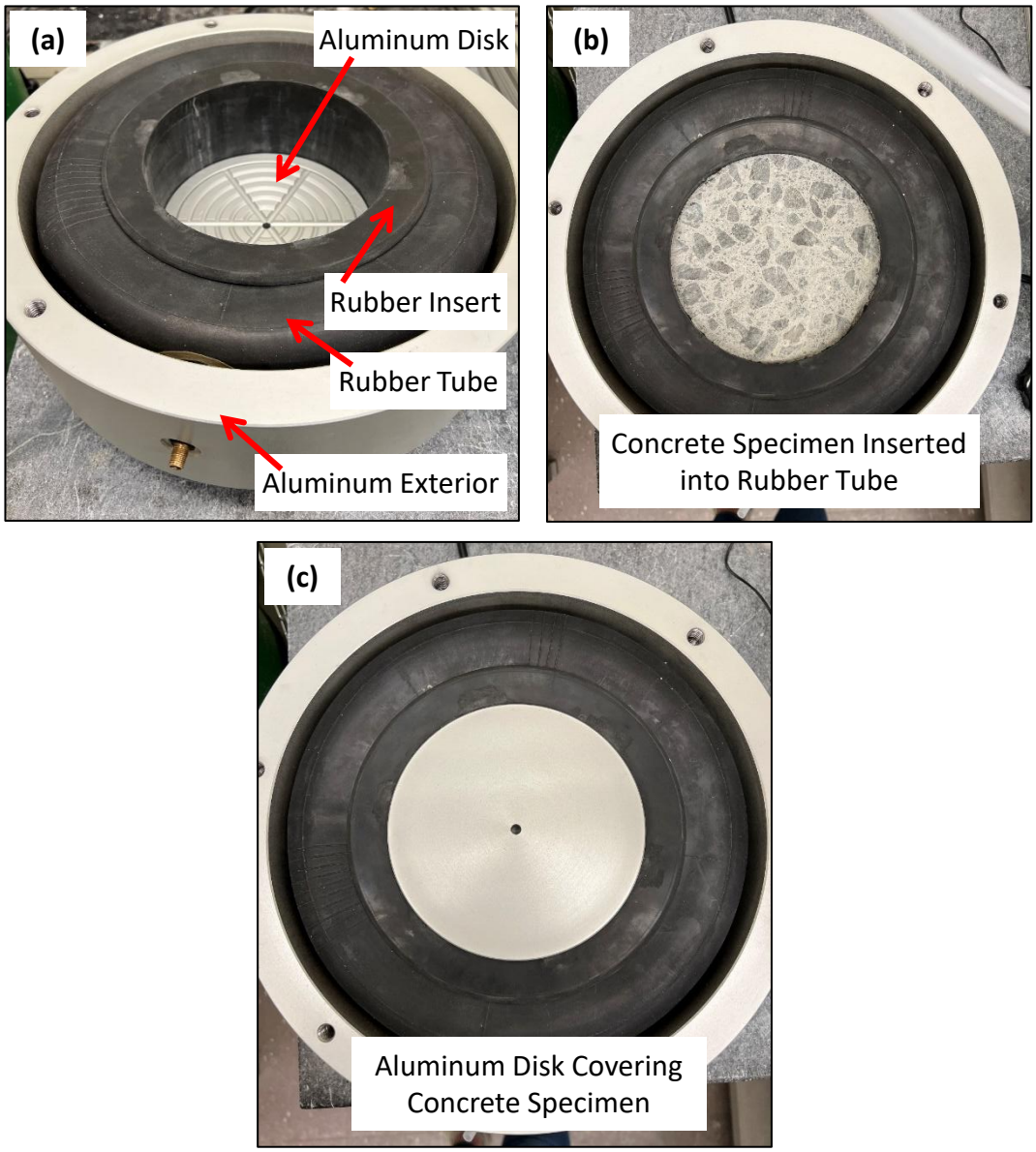

Figure 6. Placing concrete specimen into permeameter cell

Once the specimen was in the permeameter cell and the lid was securely attached, the rubber tube could be inflated to induce one-dimensional air flow through the specimen. The manufacturer recommended inflating the tube to a pressure of 950 kPa (137 psi). Although there is compressed air in the laboratory where the equipment was located, the pressure only reached 689 kPa (100 psi) which was not sufficient for filling the tube. Therefore, an air compressor rated for pressures up to 965 kPa (140 psi) was used to inflate the tube (Figure 7a). To facilitate inflation of the rubber tire, an extender could be attached to the tube's valve stem to give the operator more room (Figure 7b). A tire inflation gun with a dial gauge was used to ensure the tube was not over inflated (Figure 7c).

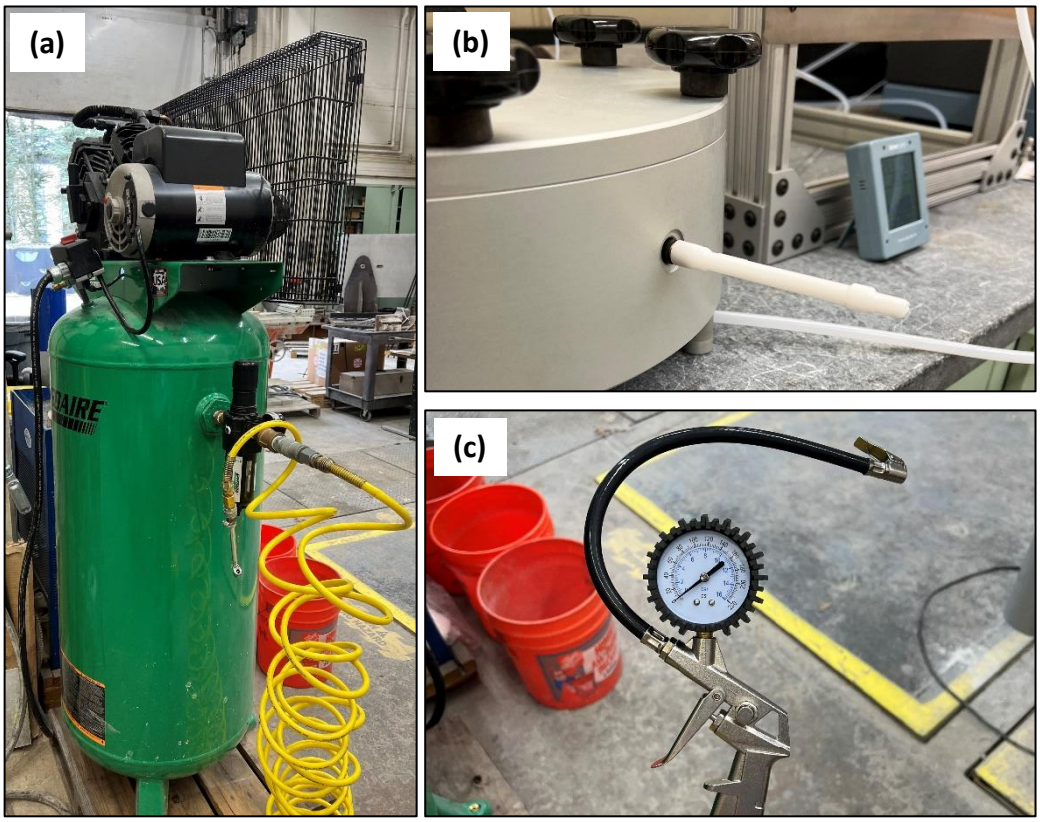

Figure 7. Rubber tube inflation: (a) 965 kPa capacity air compressor; (b) valve stem extender; (c) inflation gun with gauge

After the rubber tube was inflated, testing of the specimen could commence. Hard nylon plastic tubing was used to connect all the equipment for testing. At the start of testing, temperature and atmospheric pressure in the laboratory were recorded using a digital thermometer and barometer. A total of five target input pressures were selected for testing: 1.5×10^5 Pa, 2.0×10^5 Pa, 2.5×10^5 Pa, 3.0×10^5 Pa, and 3.5×10^5 Pa. At each target input pressure, a steady-state flow was measured prior to moving to the next pressure. Once a steady-state flow was measured at all pressures, the test was considered complete. The oxygen cylinder was closed to ensure oxygen was not actively flowing through the specimen. The rubber tube was deflated, and then the permeameter cell lid could be taken off and the specimen could be removed.

Although the air permeability cell is designed to test 152.4 mm diameter specimens, two sets of neoprene rings were manufactured to allow for the testing of 101.6 mm diameter specimens (Goal 2 of this study). Rubber inserts were designed to have an outer diameter of 152.4 mm and an inner diameter of 101.6 mm and a height of approximately 50 mm (Figure 8). Since 50 mm pieces of neoprene rubber were difficult to source, it was decided to use a 25 mm (1-inch) piece of neoprene rubber and machine two 25 mm inserts that would stack atop one another around a concrete specimen.

A 914 mm wide by 305 mm long by 25 mm thick (36-inch wide by 12-inch long by 1-inch thick) sheet of multipurpose 50A durometer neoprene (McMaster-Carr) was purchased from and machined at NIST using a waterjet (Figure 9). This durometer was chosen as it was flexible enough

to allow for the inserts to be placed around the concrete, but not so flexible that the insert would snap and/or break.

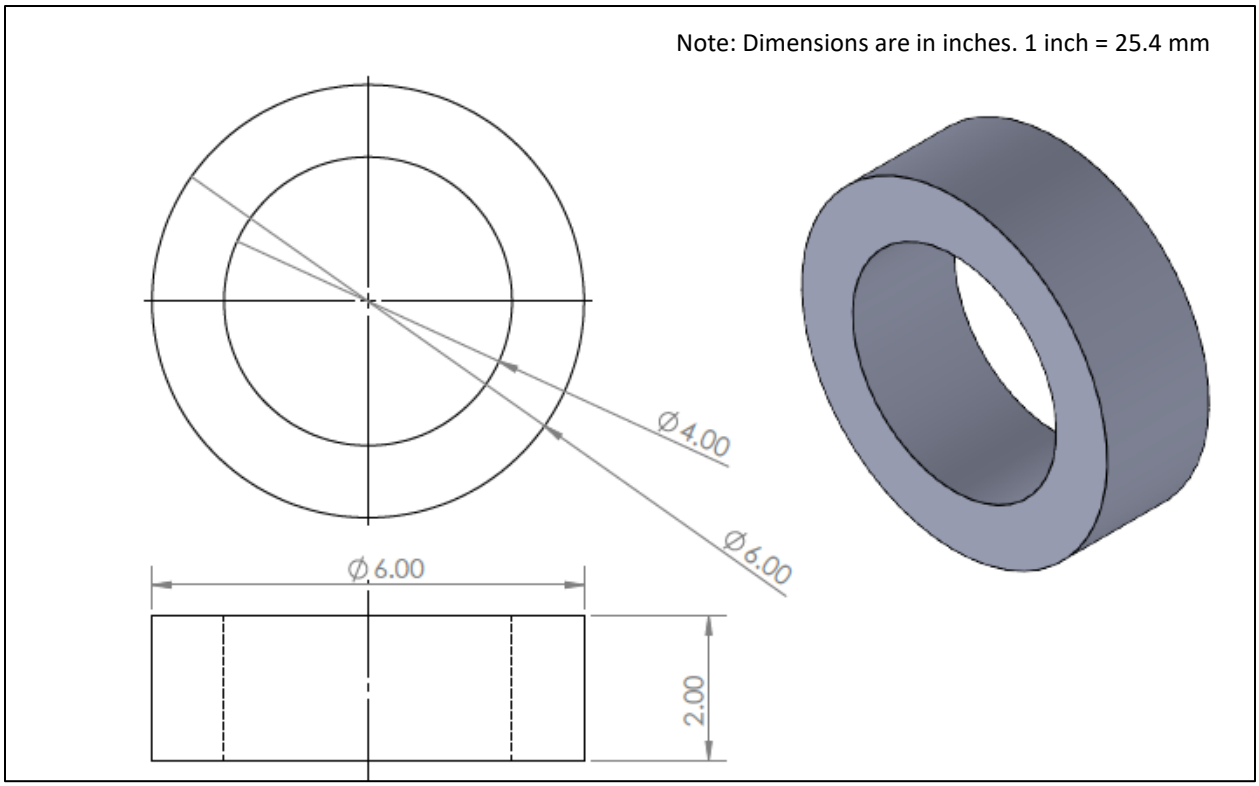

Figure 8. Schematic of rubber inserts designed for testing of 4-inch diameter concrete specimens in air permeability cell

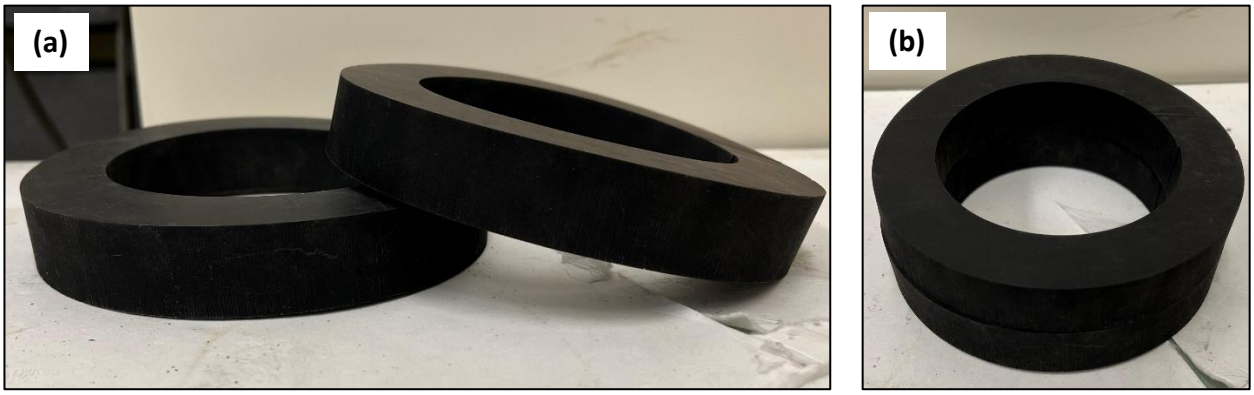

Figure 9. Machined neoprene inserts: (a) side view of two machined inserts; (b) two inserts stacked for testing

3. Validation of Air Permeability Equipment for 152.4 mm (6-inch) Diameter Specimens

As detailed in Figure 3, efforts to validate the air permeability equipment for 152.4 mm (6-inch) diameter concrete specimens focused on two key objectives. To meet these objectives, the various aspects of the equipment were studied as summarized in Table 2.

Table 2. Summary of Goal 1 objectives and corresponding experiments

Objective	Experiments
1 – accuracy of as-received equipment and testing protocols	A – flow rate measurement method B – minimum tube pressure to stop blow by C – preconditioning protocols
2 – validation of expected trends using finalized testing protocols	A – measurement repeatability B – w/cm ratio trends C – sealant trends

3.1. Materials and Specimen Preparation

To evaluate the air permeability set-up, concretes with water to cementitious materials ratios (w/cm) of 0.45, 0.55, and 0.65 were chosen for this phase of the study. Table 3 summarizes the materials used as well as the developed mixture design for each target w/cm ratio. The ASTM C150 Type I/II cement had a specific gravity of 3.15. The ASTM C778 graded sand had a specific gravity of approximately 2.6 and absorption of 0.5 %. The ASTM C33 #57 aggregate was of diabase mineralogy with a specific gravity of 3.0 and an absorption of 1 %. All aggregate was oven-dried at 110 °C for a minimum of 24 hours prior to mixing.

Table 3. Concrete materials and mix design used for validation of 152.4 mm (6-inch) diameter cores

Constituent	Description	Mix Design (kg/m^3) [lb/yd^3]		
		0.45 w/cm	0.55 w/cm	0.65 w/cm
Cement	ASTM C150 Type I/II	(428) [722]	(351) [591]	(297) [500]
Fine Aggregate	ASTM C778 Graded Sand	(743) [1252]	(809) [1363]	(854) [1440]
Coarse Aggregate	ASTM C33 #57 Diabase	(1105) [1863]	(1105) [1863]	(1105) [1863]
Water	Potable; Tap	(204) [344]	(204) [344]	(204) [344]

In total, five 0.006 m^3 (0.22 ft^3) batches of concrete were mixed: one 0.65 w/cm ratio batch; one 0.55 w/cm ratio batch; and three 0.45 w/cm ratio batches. Each batch of concrete was mixed in a 0.02 m^3 (0.67 ft^3) capacity bucket mixer following mixing protocols outlined in ASTM C192 (Figure 10a). After mixing each batch, one 15.2 cm (6-inch) diameter by 30.5 cm (12-inch) tall cylindrical specimen was cast. After 24 hours, all five specimens were demolded, labeled, and placed into a curing chamber kept at approximately 23 °C and a relative humidity of 100% for seven days (Figure 10b). After seven days of curing, specimens were removed and wet cut into three 5.1 cm (2-inch) pucks using a masonry block saw (Figure 10c). Once cut, pucks were dried at room temperature in a conditioned laboratory space to remove surface moisture from the wet saw.

Two sets of 0.45 w/cm ratio pucks were sealed with two commercially available sealants, a two-part polyurethane and a lithium silicate-based sealant, to evaluate the potential of the

equipment to differentiate between sealed concretes (Figure 10d). These sealants were selected as they have different mitigation mechanisms and therefore could have varying air permeability. Both sealants were manually applied to specimens in one coat using a paint brush. All specimens were sealed in a fume hood and left in the hood for one week to allow for full sealant curing prior to any testing.

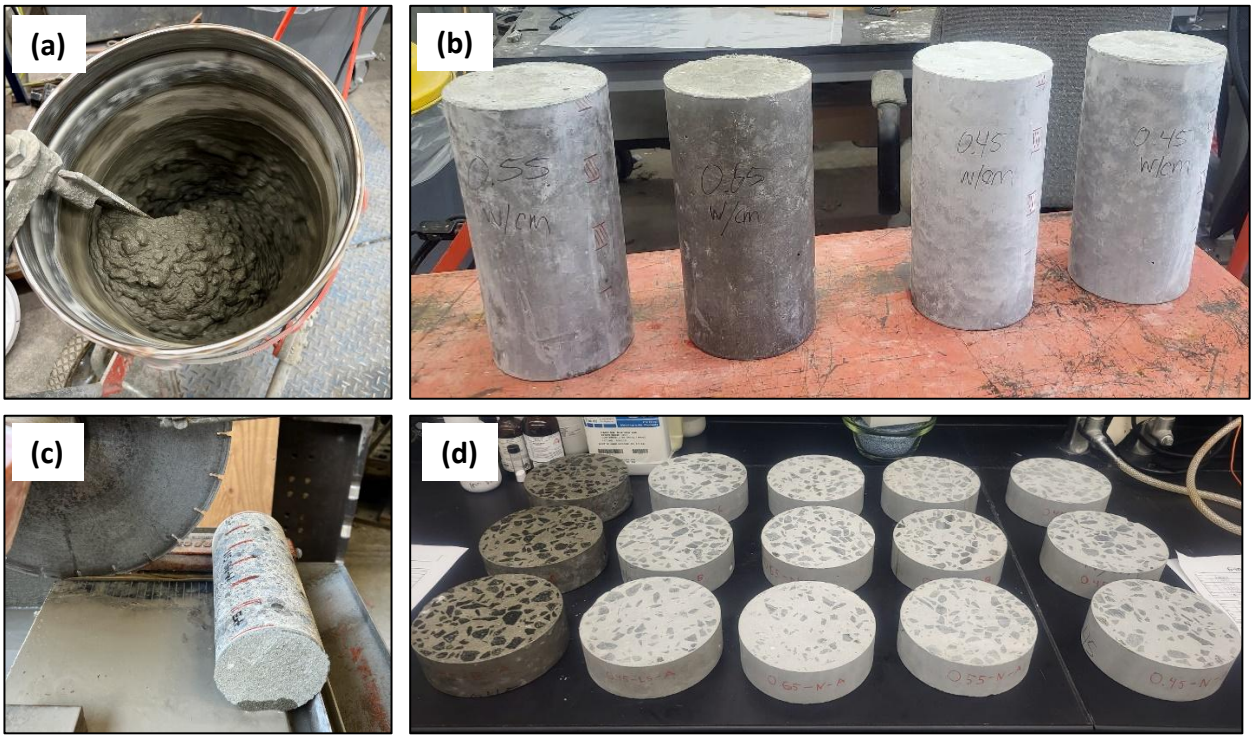

Figure 10. Mixing and specimen preparation: (a) fresh concrete in 0.02 m^2 bucket mixer; (b) cast 15.2 cm by 30.5 cm specimens of varying w/cm ratios; (c) cutting specimens with masonry block saw; (d) sealed and unsealed pucks ready for testing

3.2. Results

3.2.1. Objective 1; Experiment A – Flow Rate Measurement Method

Objective 1 Experiment A aims to evaluate the manufacturer method of measuring volumetric flow rate with soap bubble flow meters against an alternative method using a digital flow meter. Inherent variability has been reported with soap bubble flow meter measurements, and as such, a digital flow meter was investigated to reduce potential variability in volumetric flow rate measurements. When using soap bubble flow meters, an operator must manually time the duration of time for a soap bubble to travel a defined distance. Using the recorded time and known traveled distance, volumetric flow rate of the air permeating the concrete specimen can be calculated using Equation 3. This manual parameter reporting introduces more opportunities for measurements to be dependent on the user.

$$Q = \frac{S_{fm} \cdot L_{fm}}{t_F - t_I} \quad \text{(Eq. 3)}$$

Where:

Q is volumetric flow rate [m^3/s]

S_{fm} is cross-sectional area of the flow meter [m^2]

L_{fm} is the reference length of the flow meter [m]

t_F is the time which the soap bubble has finishes the reference length [s]

t_I is the time which the soap bubble begins traveling the reference length [s]

In these experiments, a concrete puck with a w/cm ratio of 0.55 was tested three times using the soap bubble flow meter, which was wetted prior to use, and the digital flow meter, respectively. The specimen remained in the air permeability cell for the duration of Experiment A, and the rubber tube was not deflated, ensuring the lateral pressure around the specimen was comparable for all tests. In addition to comparing the two flow rate measurement techniques, replication allowed for the variability of flow rate measurements to be evaluated.

Figure 11 shows the average permeability calculated using Equation 1 as a function of absolute pressure for each flow rate measurement method. Each point on the plot is an average of three measured flow rates and its associated standard deviation. Overall, the primary differences in the recorded permeability appear to be at lower inlet pressures. Standard deviation is also larger for the soap bubble flow meter compared to the digital flow meter. This is likely due to variable nature of the soap bubble meter that relies on the operator to accurately record the time for the bubble to move the required distance. However, the digital flow meter has little to no variability in average permeability values indicating it is much more consistent from test to test. Based on these findings, the digital flow meter was adopted as the default volumetric flow rate measurement method going forward.

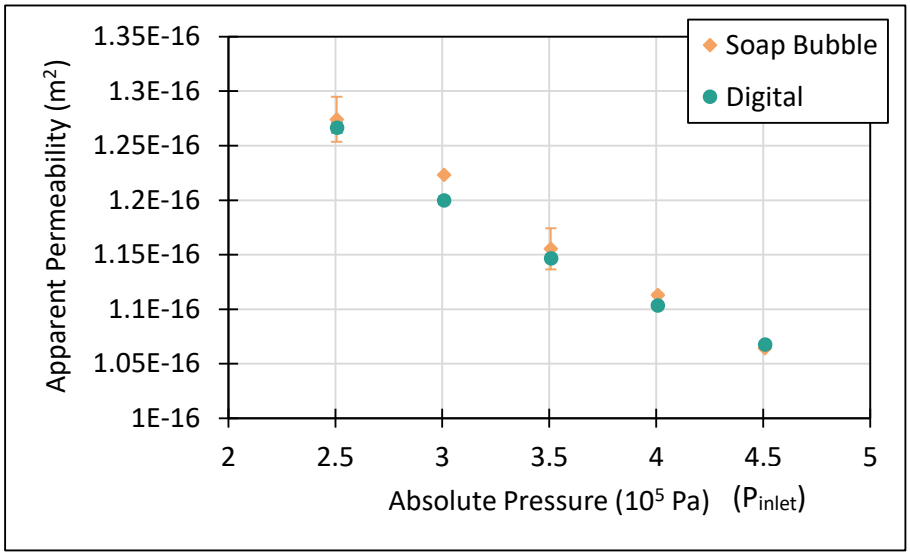

Figure 11. Comparison of apparent permeability calculated using soap bubble and digital flow meters

3.2.2. Objective 1; Experiment B – Minimum Rubber Tube Inflation Pressure

Objective 1 Experiment B quantifies the minimum rubber tube inflation pressure needed to achieve lateral confinement and facilitate one-dimensional air flow through the concrete specimen. From a theoretical perspective, the influence of lateral confining pressure can be described using Figure 12. If the confining lateral pressure around the specimen is too low, then air will be able to go around rather than through the specimen which will result in apparent permeability measurements that are uncharacteristically high. This phenomenon is known as "blow-by". As the lateral confining pressure increases, it reaches a point where there is sufficient lateral confinement, and air is permeating through the specimen with no blow-by. This is the desired range for lateral confining pressure. If lateral pressure were to continue to increase, the pore structure of the specimen would become affected as the specimen was pushed together to a point where no air could permeate the specimen. It should be noted that this final stage of lateral confinement cannot be reached using the equipment discussed herein. The equipment has an engineering control such that a specific pressure rating for the rubber tube will result in tube failure before crushing a specimen.

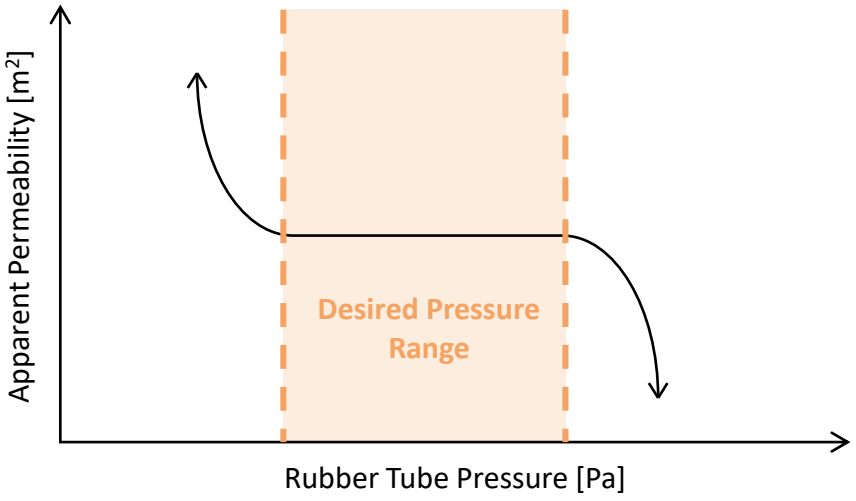

Figure 12. Theoretical relationship between rubber tube pressure and apparent permeability

Experiments were conducted at a range of rubber tube pressures using concrete specimens with a 0.45 and 0.55 w/cm ratio. During these experiments, a concrete specimen was placed in the air permeability cell and was not removed until all confining pressures of interest were tested. For the first test in a series, the rubber tube was inflated to the lowest target pressure; during each subsequent test, the rubber tube was inflated to the next target pressure until all target rubber tube pressures were reached. It should be noted that target pressures are designated by the standard, but NIST added more intervals (2.5 and 3.5) for completeness.

Figure 13 shows the trends for permeability as a function of tube pressure for 0.45 w/cm and 0.55 w/cm ratio specimens at each of the five inlet pressures (P_{in}) defined by the experimental protocol. At lower inlet pressures, there is a weak trend between the influence of lateral confinement and tube pressure, and the data scatter is high, especially for lower w/cm ratio specimens. As inlet pressures increase to 3.0×10^5 Pa and 3.5×10^5 Pa, a clear decreasing

trend is present. For 0.45 w/cm ratio specimens, a minimum rubber tube pressure of approximately 860 kPa (125 psi) is required to obtain a consistent permeability reading and mitigate the effects of blow-by; however, for the 0.55 w/cm ratio specimen, this minimum tube pressure is approximately 895 kPa (130 psi). Based on these findings and the limitations of the equipment used for air permeability testing, a minimum tube pressure of 860 kPa (125 psi) is recommended for all experiments.

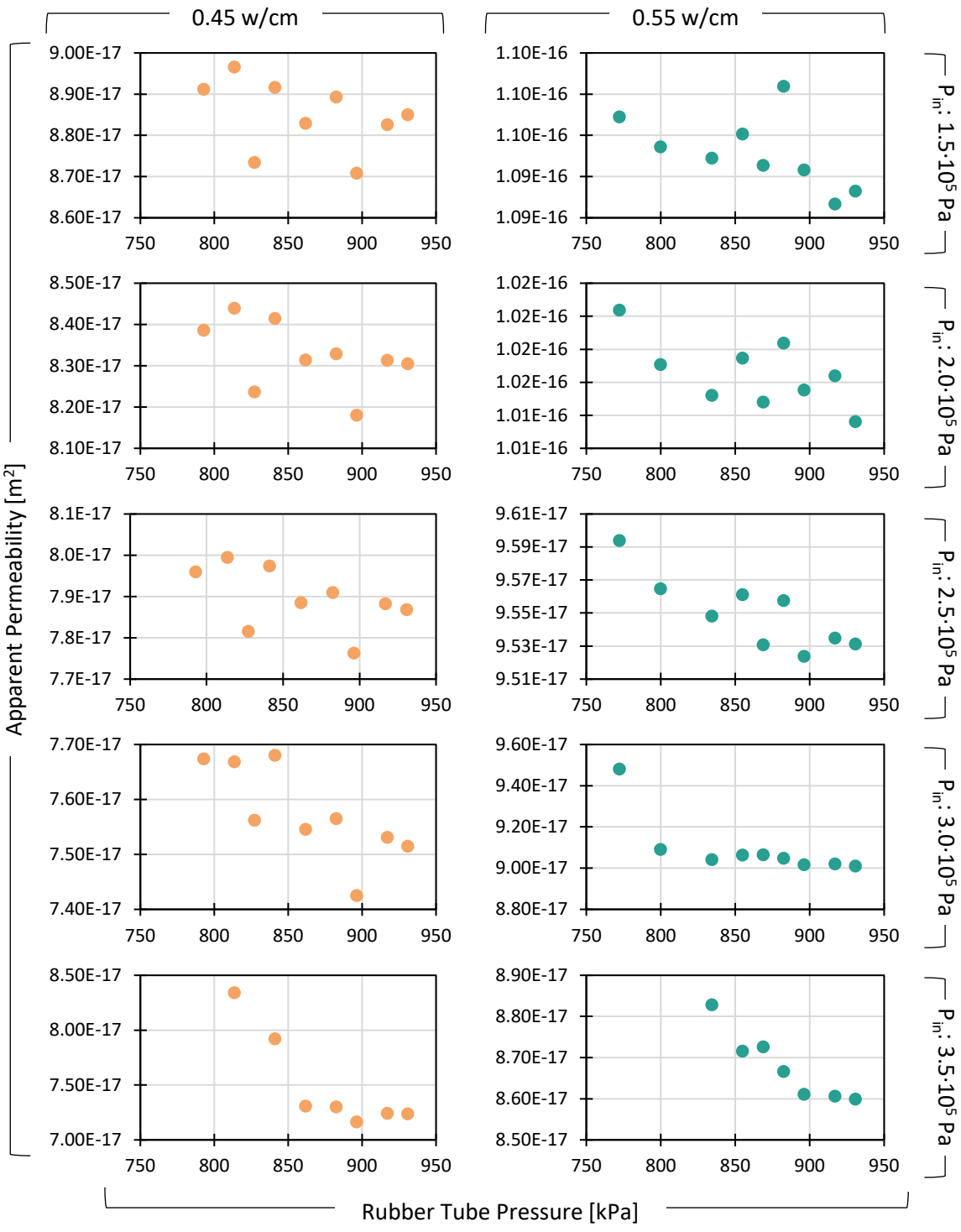

Figure 13. Influence of rubber tube pressure on measured air permeability

3.2.3. Objective 1; Experiment C – Preconditioning Protocols

Objective 1 Experiment C aimed to quantify the effects of different preconditioning protocols on air permeability readings to determine the best method to use for all tests.

Literature has clearly defined the inverse relationship between concrete moisture content and air permeability readings [22]. When developing the initial RILEM-Cembureau permeability methodology, TC 116 presented two different preconditioning protocols to ensure that moisture content was considered prior to testing for air permeability. The first recommended protocol was to condition specimens in a 20 °C, 65 % relative humidity environment for 28-days to minimize the internal moisture gradient. The second recommended protocol was to dry specimens in a chamber set to 50 °C, 10 % relative humidity to reach an equilibrium moisture content. Once equilibrium was achieved, specimens were kept in a sealed container and exposed to a saturated salt solution to achieve an ambient humidity of 75 % for 28-days.

In this study, concrete specimens with a w/cm ratio of 0.45 were treated following two preconditioning protocols. For preconditioning protocol 1, specimens oven dried for 24 hours at 110 °C and then allowed to cool to room temperature on a lab bench for approximately 1 to 2 weeks prior to testing. In preconditioning protocol 2, specimens were oven dried for 24 hours at 110 °C and then cooled in a sealed desiccator until the time of testing. Although neither method is realistic of in-situ moisture conditions in a concrete structure, oven drying to an approximate moisture content of zero was deemed as the most consistent method to achieve comparable moisture contents in a range of concrete specimens, thus ensuring that comparisons of air permeability could be drawn between different groups of specimens.

Figure 14 visualizes the differences in air permeability due to the preconditioning protocol. As expected, apparent permeability of the desiccator cooled specimens was higher than the air-cooled specimens. Standard deviation was also higher for specimens that underwent desiccator cooling, but this error can be associated with several other aspects of the testing protocol (e.g., rubber tire pressure) and is not simply a function of preconditioning method alone. During the cooling stage, specimens undergoing counter cooling absorbed water from the laboratory air; however, the exact amount of water is unknown. Additionally, the humidity in the laboratory spaces is variable which could lead to a different amount of moisture being absorbed during any one test. As a result, it was chosen that experimental testing should utilize oven drying followed by desiccator cooling to ensure moisture content of specimens is negligible until the desired testing time.

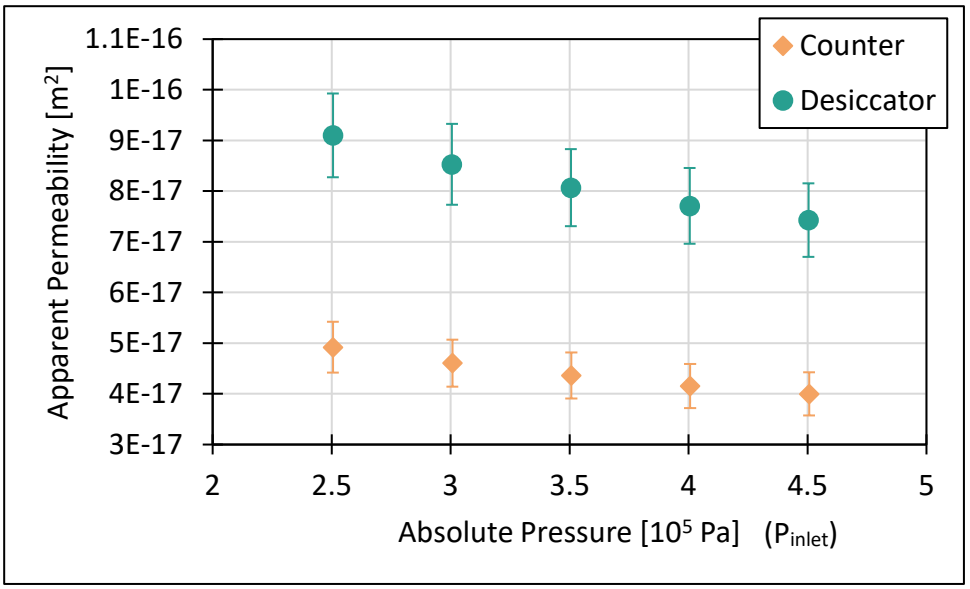

Figure 14. Comparison of preconditioning methods for air permeability measurements

3.2.4. Objective 2; Experiment A – Repeatability of Testing Protocol

Objective 2 Experiment A quantified the repeatability of air permeability measurements on one specimen. To meet this objective, one puck of each w/cm ratio was tested either two or three times over a period of several weeks. Prior to the first test, specimens were oven dried and then counter cooled in a temperature-controlled laboratory. Between each test, specimens were kept in a laboratory space that was temperature controlled and kept around 23 °C.

Figure 15 presents repeatability trends for three different w/cm ratio specimens. The variability between apparent permeability (k_A) at each absolute pressure was evaluated by comparing the range of measured k_A values, denoted as Δk_A. Generally, variability of air permeability measurements tends to decrease as absolute pressure increases. When a specimen is exposed to higher inlet pressures, slippage flow decreases indicating the measured apparent permeability (k_A) is closer to the intrinsic permeability (k_0) of the concrete [18, 23]. Permeability measurement variability also decreased since the measured apparent permeability values were closer to the intrinsic material value leaving less room for deviations. Additionally, w/cm ratio also had a noticeable effect on the variability of apparent permeability measurements. Increases in w/cm ratio created a more porous concrete, which can lead to increased slippage when measuring permeability. Although there were noticeable trends in the variability of apparent permeability values, Δk_A values were typically 1 to 2 orders of magnitude less than the measured apparent permeability. This indicates good equipment repeatability, especially when the same operator performs all testing.

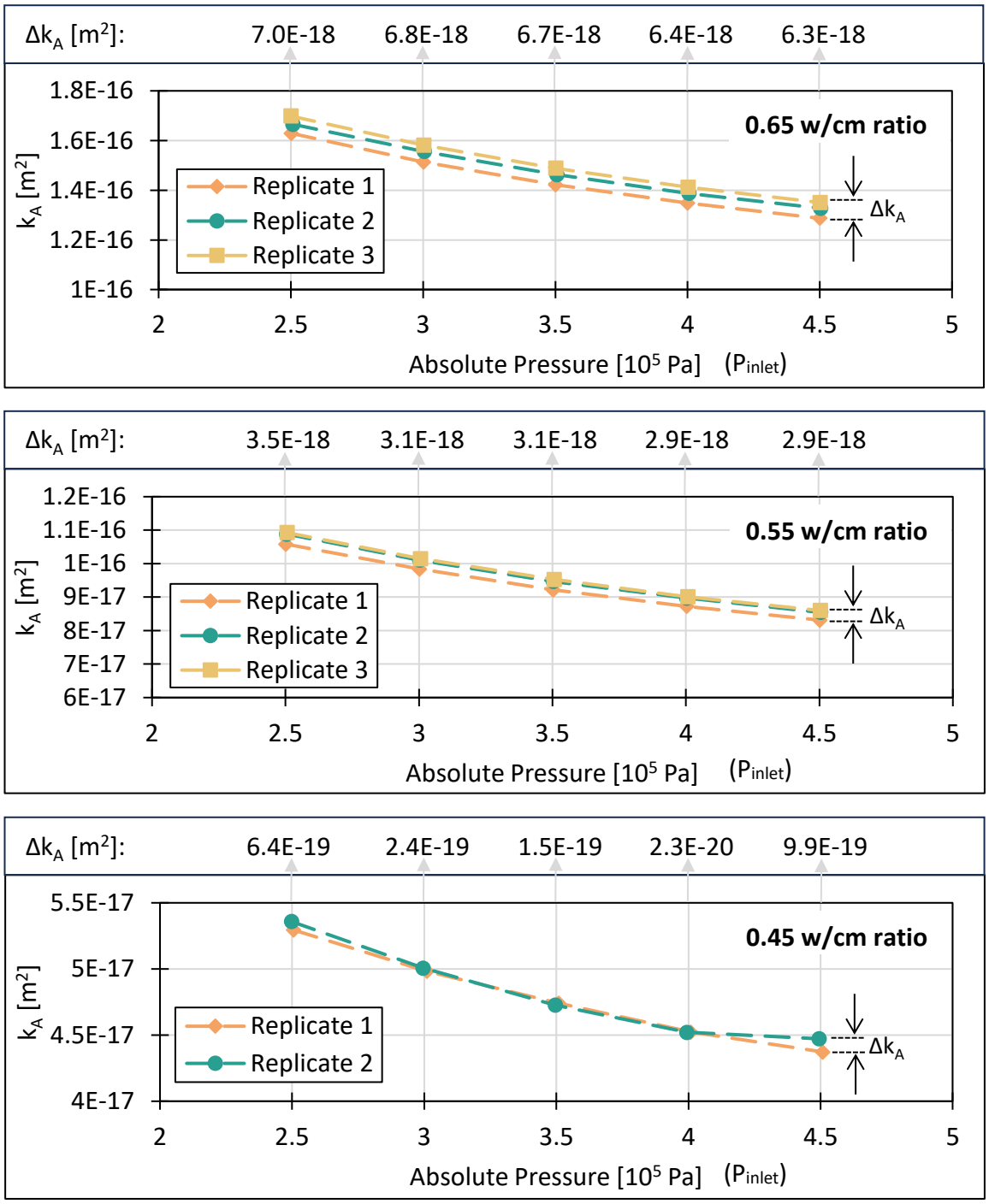

Figure 15. Repeatability of air permeability measurements on a single specimen

3.2.5. Objective 2; Experiment B – w/cm Ratio Trends

Objective 2 Experiment B focused on evaluating air permeability trends of concrete specimens with varying w/cm ratios. As mentioned in the previous section, the w/cm ratio is directly linked to the permeability of concrete due to its influence on pore size and distribution

as well as pore connectivity [24, 25]. As individual concrete ingredients are mixed, water reacts with cement to form hydration products, most notably calcium silicate hydrate (CSH). Excess mixing water remains in the matrix until it is either utilized in later hydration reactions or lost to evaporation. The space remaining from the bound water contributes to a concrete's pore network where water and air can move freely through the concrete. In concrete with a low w/cm ratio, this pore network can be smaller and more discontinuous, allowing for less air/water to move through the concrete.

Using the findings from Objective 1, the permeability equipment and developed testing protocols were checked to ensure expected permeability trends could be produced. Concrete pucks mixed with w/cm ratios of 0.45, 0.55, and 0.65 were used to validate the expected trend (Figure 16). As expected, with decreases in w/cm ratio, the measured air permeability also decreased. Additionally, the rate of measured permeability decrease was significantly higher at higher w/cm ratios compared to lower w/cm ratios. For the 0.65 w/cm ratio, apparent permeability decreased, on average, -1.7 x 10^{-17} m^2 for each increase of 1 x 10^5 Pa absolute pressure. However, these rates were -1.1 x 10^{-17} $m^2/10^5$ Pa for a w/cm ratio of 0.55 and -0.5 x 10^{-17} $m^2/10^5$ Pa for a w/cm ratio of 0.45. As mentioned previously, this finding is due to the interconnected nature of the pore network for concrete with a high w/cm ratio compared to the disconnected network of low w/cm ratio concrete.

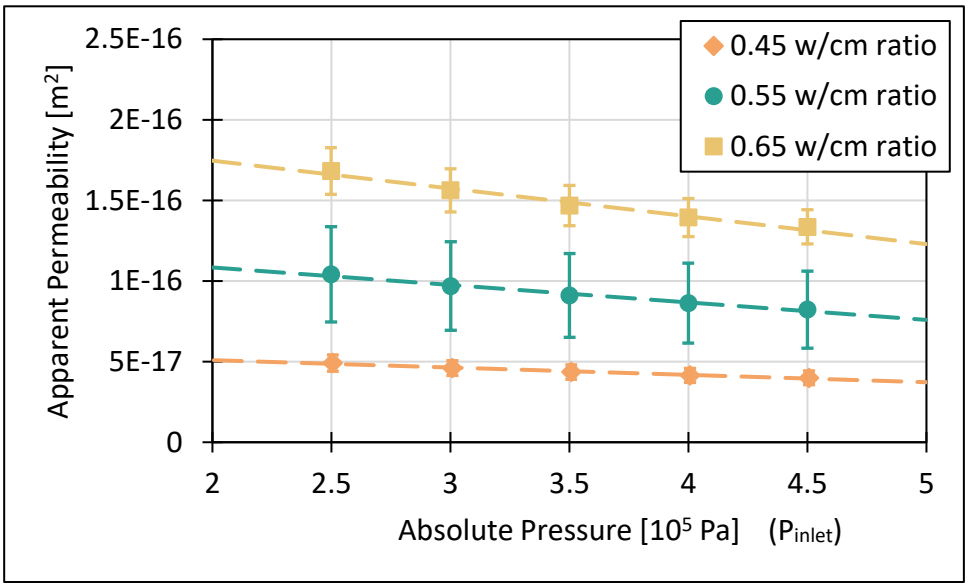

Figure 16. Measured apparent permeability as a function of concrete w/cm ratio

3.2.6. Objective 2; Experiment C – Sensitivity of Equipment to Sealants

Objective 2 Experiment C aimed to evaluate if the air permeability system could detect changes in concrete permeability due to different sealants applied to the outer surface of the puck. Several types of sealants are being evaluated at NIST as a potential mitigation technique for concrete foundations built with pyrrhotite aggregate. If sealants are to be utilized by homeowners as a mitigation strategy, it is important to ensure there are performance-based metrics that sealants must meet in order to be used. As such, initial efforts outlined in this section

are aimed at determining if potential differences in air permeability due to sealant type could be detected by the equipment.

As mentioned in Section 3.1, two sealants with distinct mitigating mechanisms were selected for this initial study. First, a lithium silicate-based sealant was selected which is categorized as an alkali-silicate pore blocking sealant. Although the exact reaction mechanism is not fully understood, it is theorized that alkalis react with portlandite (i.e., calcium hydroxide) in the cementitious matrix which precipitates CSH in the surrounding pore space and decreases permeability [16]. The second sealant was a two-part polyurethane sealant which is categorized as a coating. For a two-part polyurethane, Part A is typically a resin base while Part B is a polyfunctional amine hardener that, when mixed, cross-links to form a solid surface once cured [16]. Although polyurethane can successfully decrease permeability when applied to concrete surfaces, it is susceptible to ultraviolet light degradation, which can affect its long-term performance.

Figure 17 plots measured permeability trends for lithium silicate and polyurethane sealed specimens as well as a control that was not sealed. Overall, both sealants applied on the concrete showed noticeable improvement in air permeability; however, the degree of success was quite different. Polyurethane sealants, which form a continuous barrier, performed better than both the lithium silicate and no sealant specimens, which showed decreasing apparent permeability as a function of increasing absolute pressure. Additionally, there was minimal change in observed apparent permeability at the varying inlet pressures for polyurethane sealed specimens while there was a visible downward slope as permeability decreased with increasing inlet pressure for lithium silicate and no sealant. Overall, the air permeability equipment with the aforementioned modifications and testing protocol can differentiate between sealed and unsealed concrete specimens indicating its potential as a performance metric for sealant evaluation.

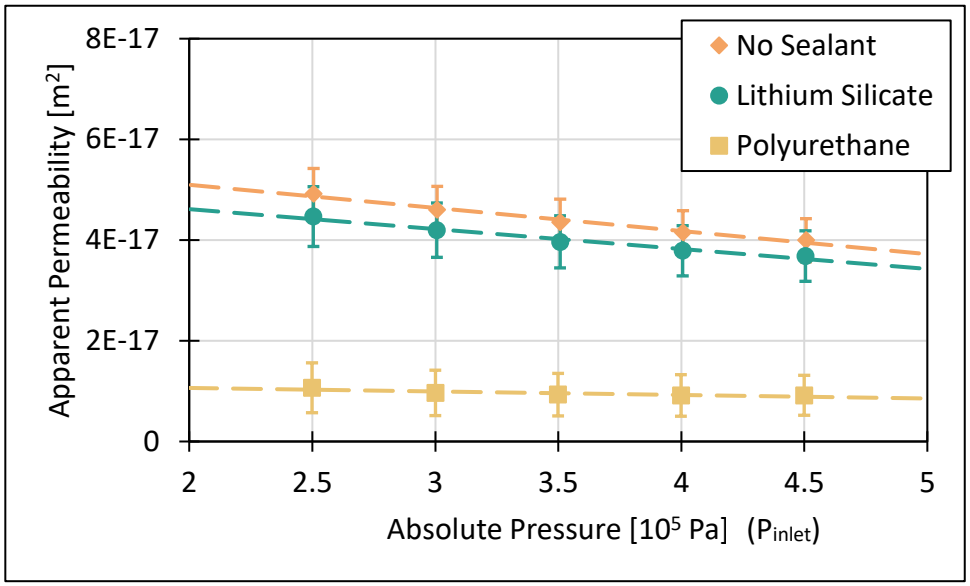

Figure 17. Measured apparent permeability for sealed concrete specimens

4. Validation of Air Permeability Equipment for 101.6 mm (4-inch) Diameter Specimens

As detailed in Figure 3, a second goal was undertaken to validate modifications made to the air permeability equipment to facilitate the testing of 101.6 mm (4-inch) diameter concrete specimens. When coring deteriorated foundations containing pyrrhotite-bearing aggregate, the typical core diameter is approximately 108 mm (4.25 inches). Therefore, the ability to test foundation cores for air permeability requires additional testing and validation. This second goal was met by focusing on the following two objectives: 1) validation of a modified testing set-up and machined parts for testing 101.6 mm diameter specimens, and 2) accuracy of air permeability measurements for specimens with heights less than 50 mm (2-inches), a height specified to capture a representative volumetric fraction of whole aggregate rocks within the cement matrix of a concrete core.

4.1. Materials and Specimen Preparation

To evaluate the air permeability modifications, concretes with water to cementitious materials ratios (w/cm) of 0.45, 0.55, and 0.65 were selected to evaluate equipment performance for a range of potential concretes. Identical concrete mixes were used to prepare both 152.4 mm and 101.6 mm specimens. Table 44 summarizes the materials used as well as the developed mixture design for each target w/cm ratio. The ASTM C595 Type IL cement had a specific gravity of 3.15 and 10 % interground limestone. The fine and coarse aggregate met the grading requirements outlined in ASTM C33 for concrete sand and #57 stone, respectively. Both aggregates were of a carbonate mineralogy where the sand was dolostone (calcium magnesium carbonate) and the crushed stone was limestone (calcium carbonate). The dolostone concrete sand had a manufacturer reported water absorption of 0.7 % while the limestone crushed stone had a manufacturer reported water absorption of 0.4 %. All aggregate was oven-dried at 110 °C for a minimum of 24 hours prior to mixing.

Table 4. Concrete materials and mix design used for validation of 101.6 mm (4-inch) diameter cores

Constituent	Description	Mix Design (kg/m^3) [lb/yd^3]		
		0.45 w/cm	0.55 w/cm	0.65 w/cm
Cement	ASTM C595 - Type IL	(455) [767]	(372) [627]	(315) [531]
Fine Aggregate	ASTM C33 – Concrete Sand	(743) [1252]	(809) [1363]	(854) [1440]
Coarse Aggregate	ASTM C33 - #57 Crushed Stone	(1105) [1863]	(1105) [1863]	(1105) [1863]
Water	Potable; Tap	(205) [345]	(205) [345]	(205) [345]

In total, three 0.008 m^3 (0.30 ft^3) batches of concrete were mixed: one 0.65 w/cm ratio batch, one 0.55 w/cm ratio batch, and one 0.45 w/cm ratio batch. Each batch of concrete was mixed in a 0.02 m^3 (0.67 ft^3) capacity bucket mixer following mixing protocols outlined in ASTM C192 (Figure 18a). After mixing each batch, one 15.2 cm (6-inch) diameter by 30.5 cm (12-inch) tall cylindrical specimen and one 10.2 cm (4-inch) by 20.3 cm (8-inch) cylindrical specimen were cast. Once cast, the lids to each specimen were tapped to the mold using electrical tape to mitigate moisture loss and all specimens were placed in a temperature-controlled chamber kept at 23°C for a total of 24 hours (Figure 18b). After the initial 24-hour curing period, specimens

were demolded using compressed air, labeled, and placed into a curing chamber kept at approximately 23 °C and a relative humidity of 100 % for 13 days (Figure 18c).

Figure 18. Mixing and curing process used for specimens to meet Goal 2 of study: (a) mixing concrete in bucket mixer; (b) initial 24 hour curing in sealed containers in temperature-controlled chamber; (c) room temperature, 100 % relative humidity curing chamber

After curing, each specimen was wet-cut using a masonry block saw. The target height for these specimens was 50.8 mm (2-inches); however, in some cases the heights varied meaningfully from this target height as shown in Table 5. In the case of 101 mm (4-inch) diameter specimens with a w/cm ratio of 0.45, the discrepancy in height was due to a user error when setting the saw guards prior to cutting. However, an extra specimen was cut to achieve one specimen that met the target height of 50.8 mm. All other height variations were due to the saw blade resonant movement during cutting. Once cut, specimens were dried at room temperature in a conditioned laboratory space to allow surface moisture from the wet saw to evaporate.

Table 5. Measured heights of Goal 2 specimens after initial sawing

Specimen ID	Height 1 [mm]	Height 2 [mm]	Height 3 [mm]	Height 4 [mm]	Average [mm]	Stdev [mm]
6”-0.65-A	49.00	48.18	47.88	49.45	48.63	0.73
6”-0.65-B	51.41	49.61	49.43	49.40	49.96	0.97
6”-0.65-C	50.27	49.12	51.41	53.04	50.96	1.67
4”-0.65-A	50.39	52.68	51.18	49.94	51.05	1.20
4”-0.65-B	51.03	51.61	51.56	51.54	51.44	0.27
4”-0.65-C	48.34	47.14	46.81	47.22	47.38	0.66
6”-0.55-A	50.52	51.99	53.80	53.57	52.47	1.53
6”-0.55-B	48.36	48.39	46.76	47.78	47.82	0.76
6”-0.55-C	49.71	48.03	49.81	50.42	49.49	1.02
4”-0.55-A	47.29	48.51	46.36	46.63	47.20	0.96
4”-0.55-B	46.53	46.30	46.58	46.61	46.51	0.14
4”-0.55-C	46.71	48.72	48.08	46.58	47.52	1.05
6”-0.45-A	49.53	49.81	48.51	49.20	49.26	0.56
6”-0.45-B	49.61	52.27	52.81	50.88	51.39	1.44
6”-0.45-C	53.82	54.38	50.39	51.38	52.50	1.91
4”-0.45-A	39.78	39.98	39.50	39.29	39.64	0.30
4”-0.45-B	40.06	39.67	40.23	40.21	40.04	0.26
4”-0.45-C	38.51	40.56	40.46	38.56	39.52	1.14
4”-0.45-D	50.14	50.34	51.10	51.74	50.83	0.73

Note: 1 mm = 0.039 inches

Based on the findings of Goal 1 of this study, all specimens were oven-dried prior to air permeability testing to achieve a consistent moisture content. Two days prior to testing, a set of three specimens was placed in a 110 °C oven for 24 hours to remove all internal moisture. Specimens were then removed from the oven and placed in a desiccator and cooled to room temperature for 12 to 24 hours prior to air permeability testing.

4.2. Results

4.2.1. Objective 1 – Validation of Modified Testing Set-Up for 101.6 mm Diameter Specimens

From an operational standpoint, the neoprene rings used to modify the testing diameter in the air permeameter were successful. The concrete specimen fit within the machined rings with no large gaps (Figure 19a). The outer diameter of the machined rings was approximately 3 mm too large for the permeameter which was ideal for a snugness of fit. The manufacturer provided rubber insert used for 152.4 mm concrete specimens is manufactured from a flexible material allowing for the insert to be pulled slightly around the neoprene rings ensuring a tight seal before lateral compression of the air tube (Figure 19b).

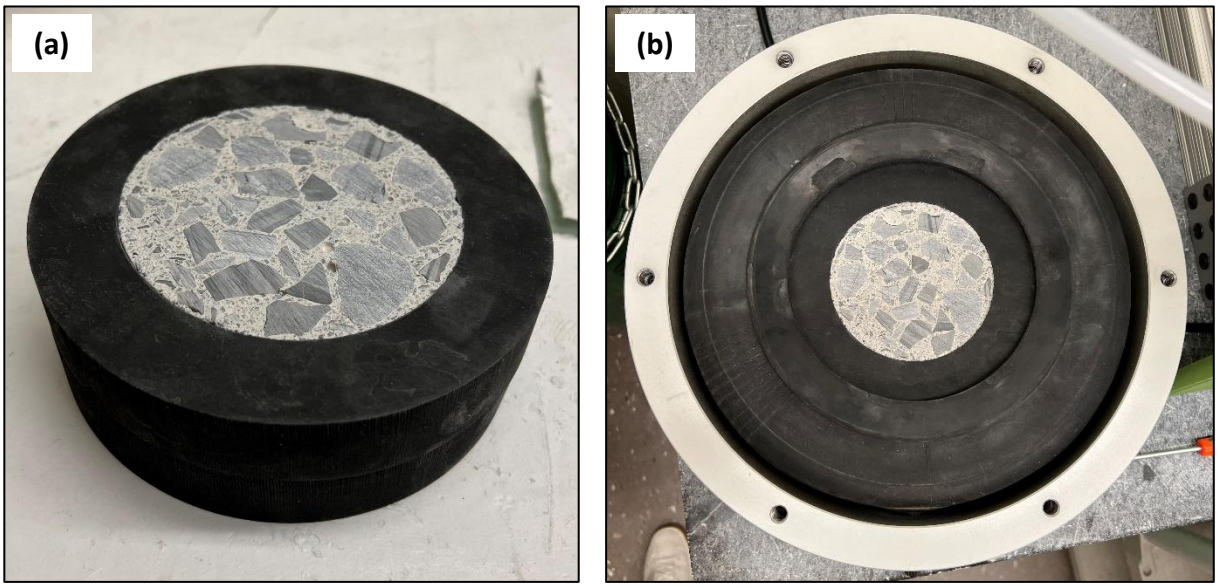

Figure 19. Manufactured neoprene rings: (a) view with 101.6 mm concrete specimen inserted; (b) 101.6 mm concrete specimen with neoprene rings in concrete air permeability cell

Figure 20 details the measured air permeability values of identically mixed 152.4 mm and 101.6 mm specimens. Generally, the 101.6 mm (4-inch) diameter specimens had a higher air permeability compared to the 152.4 mm (6-inch) diameter specimens. However, as the w/cm ratio decreased (i.e., the permeability of the concrete decreased), the differences between the measured permeability values (Δk_A) decreased. For 0.65 w/cm ratio specimens the average Δk_A was 3.00×10^{-16} with a standard deviation of 1.0×10^{-17}, 0.55 w/cm ratio specimens had an average Δk_A of 2.29×10^{-16} with a standard deviation of 2.9×10^{-18}, and 0.45 w/cm ratio specimens had an average Δk_A was 2.40×10^{-17} with a standard deviation of 4.5×10^{-18}. Although the 0.45 w/cm ratio specimens had a Δk_A that was one order of magnitude lower than the 0.55 and 0.65 w/cm ratio specimens, it was still one to two orders of magnitude higher than the reported variability of identical 152.4 mm diameter replicates in Figure 15.

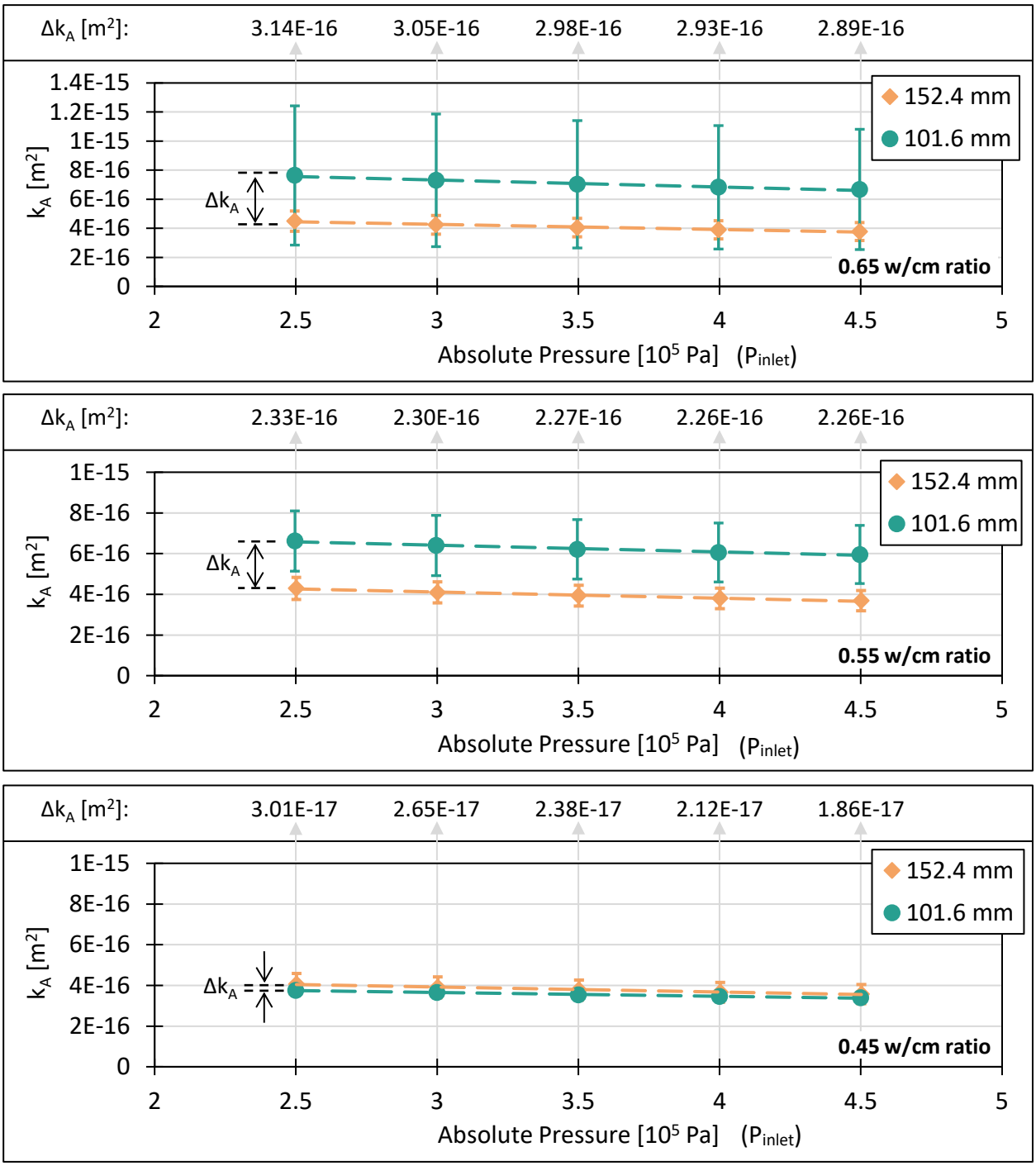

Figure 20. Comparison of measured air permeability for 152.4 mm and 101.6 mm specimens tested in the RILEM-Cembureau air permeability set-up

Statistical analysis was conducted to determine if there were statistical differences between the measured air permeability due to diameter. First, each data set was checked for normality (i.e., whether the data fit a normal data distribution) using the Anderson-Darling method at a significance level (α) of 0.05. For all w/cm ratios, the 152.4 mm diameter specimens exhibited a normal distribution (*p*-values of 0.73 and 0.97) while the 101.6 mm diameter

specimens did not exhibit a normal distribution (*p*-values of 0.001 and 0.002). As a result, the Mann-Whitney U test at a significance level of 0.05 was chosen to evaluate statistical differences between data sets since the data for the 101.6 mm specimens were determined to be non-parametric (or non-normal). The Mann-Whitney U test is the non-parametric equivalent of the more common two sample *t*-test (which is only valid for normally distributed data). For the 0.55 and 0.65 w/cm ratio specimens, the Mann-Whitney U test revealed that the 101.6 mm diameter specimens had a significantly higher measured apparent permeability (k_A) than identically cast 152.4 mm diameter specimens with *p*-values of 0.02 for 0.65 w/cm specimens and 3.1 x 10^{-6} for 0.55 w/cm ratio specimens. However, for 0.45 w/cm specimens, there was no statistically significant difference in the measured air permeability values (*p*-value of 0.24).

This result aligns with literature detailing the impact of specimen size on permeability. One study reported that for identical mixtures, cube specimens had a larger permeability than cylindrical specimens; however, for both geometries, 100 mm specimens had a significantly larger permeability than 150 mm specimens [26]. This trend can be attributed to the influence of the interfacial transition zone (ITZ) on the overall permeability of concrete. Snyder et al. [27] reported that the ITZ has larger pores than the surrounding cementitious matrix, which can lead to increased permeability. For specimens that used identically sized aggregate, a smaller specimen would have more ITZs making up the overall volume of the specimen compared to a larger specimen due in part to the smaller ratio of specimen diameter to aggregate length.

Since it is understood both through literature and experimental validation that specimen diameter can have a significant effect on the permeability of concrete, it becomes important to validate whether using the neoprene inserts to test 101.6 mm specimens yields the same permeability trends as 152.4 mm specimens. Figure 21 provides a visual of permeability trends for each specimen diameter. For both specimen sizes, the same general trend is seen where a w/cm ratio of 0.45 yielded the lowest permeability followed by 0.55 and 0.65. A statistical analysis was completed for both specimen sizes to determine if the differences in w/cm ratios were significant and if these differences were the same for both specimen sizes. A summary of the statistical tests can be found in **Error! Reference source not found.**. For the 152.4 mm diameter data, analysis of variance tests followed by Tukey's post-hoc analysis was conducted to determine the statistical differences between the w/cm ratios since the data were parametric. For the 101.6 mm diameter data, Kruskal-Wallis test followed by the Dunn-Bonferroni post-hoc analysis was conducted to determine the differences between the w/cm ratios since the data were not parametric.

Table 6. Summary of statistical analysis of w/cm ratio on permeability for each specimen size

Comparison	152.4 mm Diameter			101.6 mm Diameter		
	$Q_{calculated}$	$Q_{critical}$	Significance	$\alpha_{calculated}$	$\alpha_{corrected}$	Significance
0.45 vs 0.55	1.68E-17	5.06E-17	NSD	0.0011	0.017	SD
0.45 vs 0.65	2.93E-17	5.06E-17	NSD	0.0324	0.017	NSD
0.55 vs 0.65	1.25E-17	5.06E-17	NSD	0.9503	0.017	NSD

Notes: 152.4 mm diameter statistics were calculated using Analysis of Variance test and Tukey's post-hoc methods. 101.6 mm diameter statistics were calculated using Kruskal-Wallis tests and Dunn-Bonferroni post-hoc methods. $Q_{calculated}$ = Q-value calculated from experimental data; $Q_{critical}$

= Q-value obtained from Studentized Range Q table; $\alpha_{calculated}$= significance value calculated using experimental data; $\alpha_{corrected}$= corrected significance value using the Bonferroni correction method; NSD = not significantly different; SD = significantly different

Analysis showed that for the 152.4 mm specimens, there was no significant difference between permeability values measured for the different w/cm ratios. For the 101.6 mm diameter specimens, there was a statistically significant difference between the measured permeability of 0.45 and 0.55 w/cm ratios; however, there were no statistically significant differences for 0.45 and 0.65 as well as for 0.55 and 0.65. Although this may seem counterintuitive, Figure 21 shows that the error bars for the 0.65 w/cm ratio include the 0.45 w/cm ratio data; however, there is no overlap between the 0.55 and 0.45 permeability data.

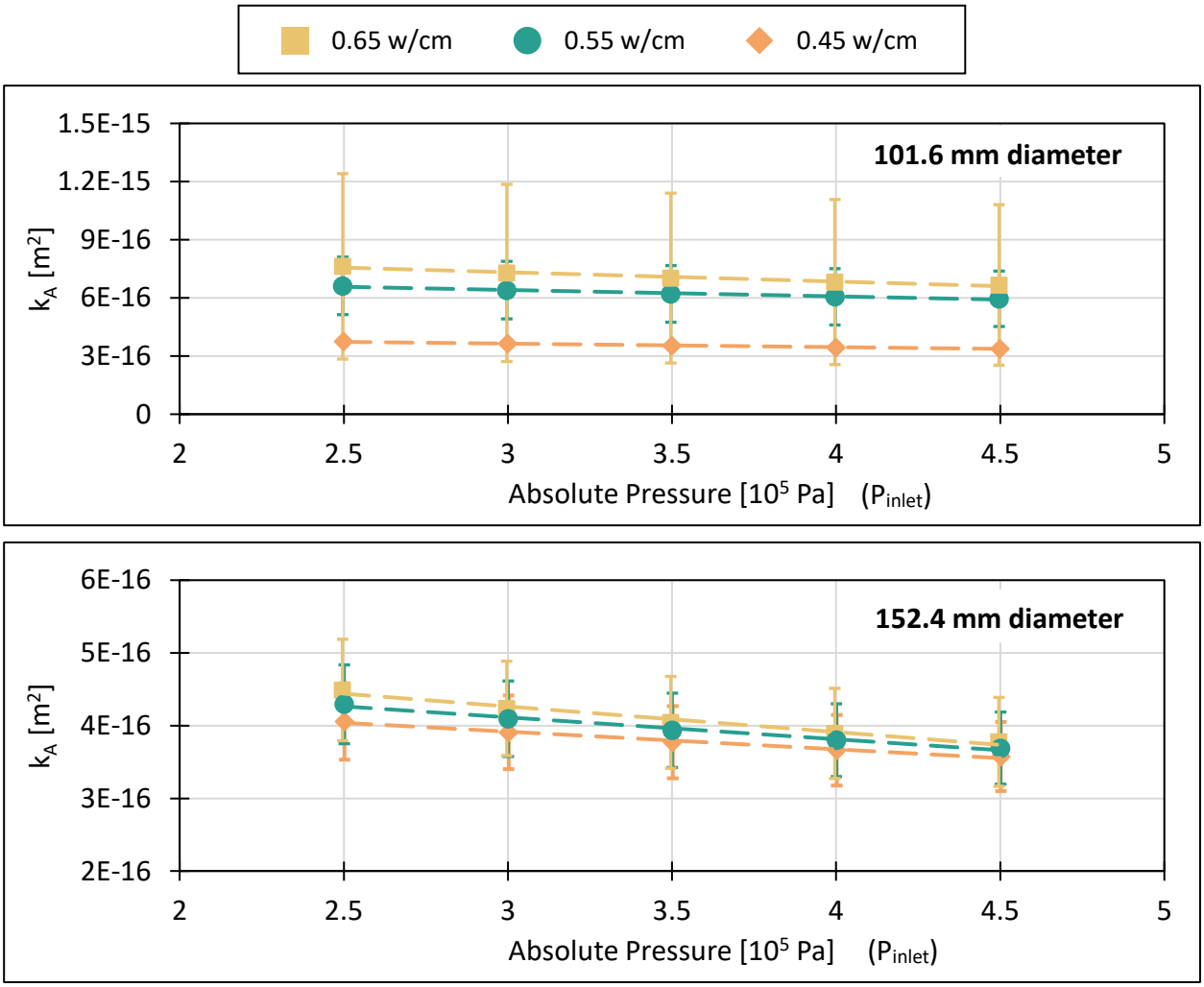

Figure 21. Comparison of air permeability trends for 152.4 mm and 101.6 mm diameter specimens

4.2.2. Objective 2 – Accuracy of Air Permeability Measurements for Specimens with Heights Less Than 50 mm

When evaluating cores from Connecticut foundations that have been affected by pyrrhotite induced damage, specimens with a height of less than 50 mm (2-inches) are commonly

cut from the core for testing due to the limited number of total field cores and the need to maximize the number of replicate specimens. The ability of the neoprene rings to evaluate specimens with a diameter of 101.6 mm and a height of less than 50 mm was of interest. Specimens with a w/cm ratio of 0.65 and 0.55 and a diameter of 101.6 mm were trimmed to a height of less than 50 mm (see Table). The 0.45 w/cm ratio specimens were not trimmed as they were initially cut to a height of 40 mm as reported in Table . The variability of the 0.65 w/cm specimens was noticeably more than the heights of other w/cm ratios.

Table 7. Measured heights of 101.6 mm diameter specimens after trimming

Specimen ID	Height 1 [mm]	Height 2 [mm]	Height 3 [mm]	Height 4 [mm]	Average [mm]	Stdev [mm]
4”-0.65-A	37.15	36.94	39.60	41.87	38.89	2.32
4”-0.65-B	38.54	40.29	40.13	38.27	39.31	1.05
4”-0.65-C	39.59	39.23	35.39	38.28	38.12	1.90
4”-0.55-A	38.77	38.37	38.79	40.46	39.10	0.93
4”-0.55-B	40.89	41.02	41.88	43.01	41.70	0.98
4”-0.55-C	40.76	38.67	40.15	41.37	40.24	1.16

Figure 22 shows a comparison of measured air permeability values of the 101.6 mm specimens with varying heights. There were noticeable differences between the two sets of specimens; however, there were no consistent trends, and the error bars from each specimen typically overlapped. Statistical analysis was used to further validate the trends between the two different heights. The Anderson-Darling test for normality was conducted on each set of data at a significance level of 0.05, and, similar to the 101.6 mm specimens with a height of 50 mm, all data sets with heights less than 50 mm were determined to be non-parametric with *p*-values of 0.003 for 0.65 w/cm, 5.3×10^{-5} for 0.55 w/cm, and 0.001 for 0.45 w/cm. Since all data sets were non-parametric, the Mann-Whitney U test was selected to determine whether there were statistically significant differences in the measured air permeability between the two specimen heights. For all three w/cm ratios evaluated, there was a statistically significant difference in measured air permeability due to specimen height with reported *p*-values of 0.04 for a w/cm of 0.65, 6.3×10^{-5} for a w/cm of 0.55, and 0.001 for a w/cm of 0.45.

There are several reasons for the statistically significant difference in measured air permeability between the specimens. It has been reported that the repeated oven drying exposure during the preconditioning process can result in anomalies [28]. The trimmed specimens were exposed to oven drying twice, once when tested at a height of 50 mm and then again after trimming. Literature clearly details that exposure to elevated temperature oven drying can lead to an increased pore structure volume due to desiccation of cement hydrates and microcrack generation from thermodynamic stresses [28]. However, this would not account for the measured trend of 0.65 w/cm ratio specimens, where the 50 mm specimens had a higher measured air permeability. This higher measured air permeability could also be the nature of the physical network of cement porosity and the distribution of aggregates resulting from concrete cure for the higher water to cement ratio. Finally, the size of aggregate and lack of inclusion of whole aggregate in the thinner specimens could enable a direct path for oxygen flow at the

interface between the cement and aggregate. Additional research is necessary to validate this hypothesis.

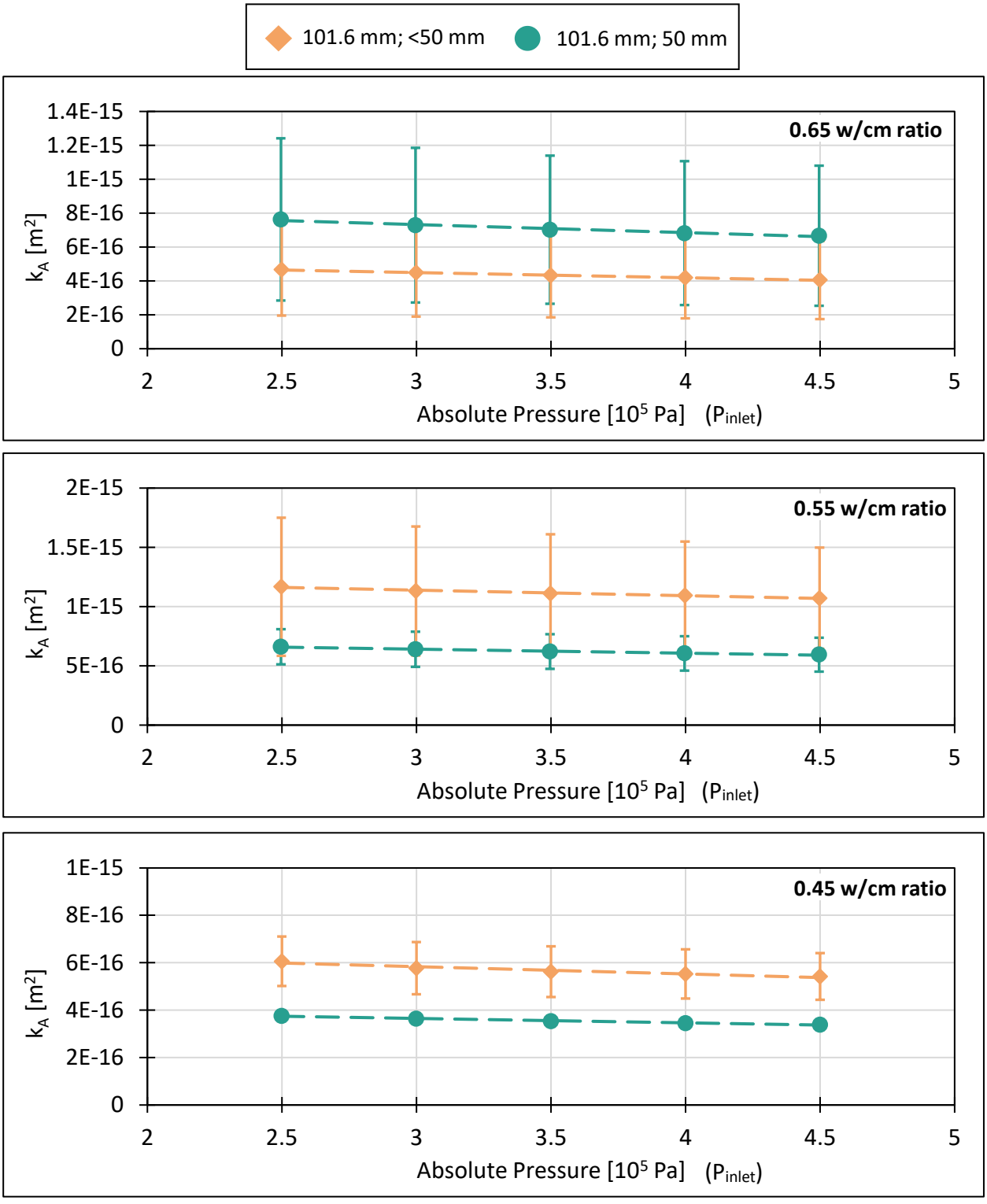

Figure 22. Comparison of measured air permeability for 101.6 mm specimens with varying heights tested in the RILEM-Cembureau air permeability set-up

5. Summary and Conclusions

In this report, a commercially available air permeability testing system was obtained to measure the air permeability of concrete specimens. To meet the first goal of this study, modifications to the as-received equipment were validated, and a testing protocol was developed to ensure consistent data was recorded. To meet the second goal of this study, additional modifications to the equipment were investigated to allow for the testing of specimens with smaller diameters and varying heights. A detailed summary of key findings and recommendations, split by study goal, is below.

5.1. Findings from Goal 1 – Validating Equipment to Test 152.4 mm Diameter Specimens

Based on the findings of the experiments reported in Chapter 3, the following modifications to the manufacture provided testing protocol are recommended:

- A digital flow meter should be used in lieu of soap bubble flow meters to remove user error and reduce variability of flow measurements.
- The rubber tube insert should be inflated to a minimum of 860 kPa (125 psi) to minimize blow by and obtain consistent flow measurements.
- Prior to testing, all specimens should be oven dried at 110 °C in order to achieve a consistent moisture state in the concrete that facilitates a reliable comparison of different concrete specimens.

In addition to the recommended modifications, the following general trends and findings were found with respect to the implementation of the air permeability equipment.

- The air permeability equipment yielded consistently measured air permeability values. For specimens tested multiple times, the variability of measured air permeability measurements at any one inlet pressure were 1 to 2 orders of magnitude less than the measured apparent air permeability.
- Decreases in concrete w/cm ratio yielded decreases in measured air permeability as w/cm ratios of 0.65, 0.55, and 0.45 reported average measured permeability values of 1.49×10^{-16} m^2, 9.21×10^{-17} m^2, and 4.41×10^{-16} m^2, respectively.
- The air permeability equipment and associated procedures were capable of detecting differences in the measured air permeability of sealed concretes; therefore, this method has the potential to serve as a performance metric in the evaluation of sealed concrete and should be introduced into current standards.

5.2. Findings from Goal 2 – Retrofitting Equipment to Test 101.6 mm Diameter Specimens

Based on the experiments reported in Chapter 4, the following trends in measured air permeability as a function of specimen diameter and height were observed.

- The manufactured neoprene rings were physically capable of working within the footprint of the existing air permeability equipment to facilitate testing of 101.6 mm diameter specimens in the 152.4 mm permeability cell.
- For increased w/cm ratios, specimens with a diameter of 101.6 mm reported measured air permeability values that were, on average, 3.00 x 10^{-16} m^2 (0.65 w/cm) and 2.29 x 10^{-16} m^2 (0.55 w/cm) higher than identically cast and cured 152.4 mm diameter specimens. However, for 0.45 w/cm specimens there was no significant difference between the measurements.
- The variability of measured air permeability values for 101.6 mm diameter specimens was typically one order of magnitude larger than identical 152.4 mm specimens. For 0.65 w/cm, the average standard deviations were 6.42 x 10^{-17} m^2 for 152.4 mm specimens versus 4.42 x 10^{-16} m^2 for 101.6 mm specimens, while for 0.55 w/cm, average standard deviations were 5.14 x 10^{-17} m^2 for 152.4 mm specimens versus 1.46 x 10^{-16} m^2 for 101.6 mm specimens.
- When varying specimen height, the trends were mixed with no clear relationship between measured air permeability and specimen height. More testing is needed, with specimens cut to a more consistent height across specimens to reduce measurement variability.
- A primary takeaway of Goal 2 is that as the specimen dimensions and testing equipment deviate from the original protocols, the likelihood of error and variability being introduced into the measurements is increased.

References

[1] Jana D (2022) Cracking of Residential Concrete Foundations in Eastern Connecticut, USA from Oxidation of Pyrrhotite. *Case Studies in Construction Materials* 16:e00909. https://doi.org/10.1016/j.cscm.2022.e00909

[2] Bashaw JT (2023) Connecticut's Crumbling Foundations: Legal Remedies and Legislative Responses. *Connecticut Law Review* 55(4):885-925.

[3] State of Connecticut (2021) An Act Concerning Crumbling Concrete Foundations. Substitute House Bill No. 6646, Public Act No. 21-120. https://www.cga.ct.gov/2021/act/Pa/pdf/2021PA-00120-R00HB-06646-PA.PDF

[4] Commonwealth of Massachusetts (2021) An Act Relative to Crumbling Concrete Foundations. Senate Bill No. 548. https://malegislature.gov/Bills/192/S548

[5] Bentivegna AF, Snyder A, Stacey SM (2023) Pyrrhotite in Concrete Aggregates. *Concrete International* 48(8):37-44.

[6] ASTM International (2023) *ASTM C1778-23 – Standard Guide for Reducing the Risk of Deleterious Alkali-Aggregate Reaction in Concrete* (ASTM International, West Conshohocken, PA). https://doi.org/10.1520/C1778-23

[7] Rodrigues A, Dechesne J, Fournier B, Durand B, Shehata MH, and Rivard P (2016) Evaluation Protocol for Concrete Aggregates Containing Iron Sulfide Minerals. *ACI Materials Journal* 113(3):349-359. https://doi.org/10.14359/51688828

[8] Guirguis B, Shehata MH (2017) A New Screening Test to Evaluate the Presence of Oxidizable Sulfide Minerals in Coarse Aggregates. *Construction and Building Materials* 154:1096-1104. https://doi.org/10.1016/j.conbuildmat.2017.07.198

[9] Jeyakaran T, Pornsiri N, Saengsoy W, Tangtermsirikul S (2023) Test Methods for Performance-Based Evaluation of Concrete Containing Iron Sulfide-Bearing Aggregates: Development and Application. *Results in Engineering* 18:101068. https://doi.org/10.1016/j.rineng.2023.101068

[10] Geiss CE, Gourley JR (2019) A Thermomagnetic Technique to Quantify the Risk of Internal Sulfate Attack due to Pyrrhotite. *Cement and Concrete Research* 115:1-7. https://doi.org/10.1016/j.cemconres.2018.09.010

[11] Gourley J, Geiss C (2023) Direct Pyrrhotite Testing and Map Cracking Risk Assessment using Magnetic Susceptibility and Total Sulfur Method. Presented at *ACI Fall Convention*, October 29 – November 2, Boston MA.

[12] Ward JC (1970) The Structure and Properties of Some Iron Sulphides. *Review of Pure and Applied Chemistry* 20:175-206

[13] Chinchón-Payá S, Aguado A, Chinchón S (2012) A Comparative Investigation of the Degradation of Pyrite and Pyrrhotite Under Simulated Laboratory Conditions. *Engineering Geology* 127:75-80. https://doi.org/10.1016/j.enggeo.2011.12.003

[14] Mengason, M.J., and Watson, S., "Pyrrhotite Reference Material Synthesis," NIST Technical Note (TN) NIST TN 2336. National Institute of Standards and Technology, Gaithersburg, MD, 2025. https://doi.org/10.6028/NIST.TN.2336

[15] Casanova, I.; Agullo, L.; Aguado, A. (1996) Aggregate Expansivity Due to Sulfide Oxidation – I. Reaction System and Rate Model, *Cement and Concrete Research* 26:993-998

[16] Carey AS and Watson SS (2025) Review of Potential Mitigation Methodologies for Existing Concrete Structures Containing Pyrrhotite-Bearing Aggregates. *Journal of Building Engineering*, 111:113408. https://doi.org/10.1016/j.jobe.2025.113408
[17] Zhang D, Li K (2019) Concrete Gas Permeability from Different Methods: Correlation Analysis. *Cement and Concrete Composites* 104:103379. https://doi.org/10.1016/j.cemconcomp.2019.103379
[18] Zhang J, Jin T, He Y, Wang Y, Gao Y, Zhang Y (2022) The Slippage Effect of Concrete Gas Permeability and the Influence of its Microstructure. *Construction and Building Materials* 333:127384. https://doi.org/10.1016/j.conbuildmat.2022.127384
[19] Kollek JJ (1989) The Determination of the Permeability of Concrete to Oxygen by the Cembureau Method – A Recommendation. *Materials and Structures* 22:225-230. https://doi.org/10.1007/BF02472192
[20] RILEM TC 116-PCD (1999) Test for Gas Permeability of Concrete: B. Measurement of the Gas Permeability of Concrete by the RILEM-Cembureau Method. *Materials and Structures* 32:176-178. https://doi.org/10.1007/BF02481511
[21] RILEM TC 116-PCD (1999) Concrete Durability – An Approach Towards Performance Testing. *Materials and Structures* 23:163-173. https://doi.org/10.1007/BF02481509
[22] Abbas A, Carcasses M, Ollivier JP (1999) Gas Permeability of Concrete in Relation to its Degree of Saturation. *Materials and Structures* 32:3-8. https://doi.org/10.1007/BF02480405
[23] Qian R, Shi J, Li Y, Chen W, Liu G, Liu Z, She W, and Zhang Y (2020) Investigation on Parameters Optimization for Gas Permeability Testing of Concrete: Inlet-Gas Pressure and Confining Pressure. *Construction and Building Materials* 250:118901. https://doi.org/10.1016/j.conbuildmat.2020.118901
[24] Sanjuán MA, Muñoz-Martialay R (1996) Influence of the Water/Cement Ratio on the Air Permeability of Concrete. *Journal of Materials Science* 31:2829-2832.
[25] Lafhaj Z, Goueygou M, Djerbi A, Kaczmarek M (2006) Correlation between Porosity, Permeability and Ultrasonic Parameters of Mortar with Variable Water/Cement Ratio and Water Content. *Cement and Concrete Research* 36:625-633. https://doi.org/10.1016/j.cemconres.2005.11.009
[26] Zhang Y, Li H, Abdelhady A, Yang J, and Wang H (2021) Effects of Specimen Shape and Size on the Permeability and Mechanical Properties of Porous Concrete. *Construction and Building Materials* 266:121074. https://doi.org/10.1016/j.conbuildmat.2020.121074
[27] Snyder KA, Winslow DN, Bentz DP, and Garboczi EJ (1991) Effects of Interfacial Zone Percolation on Cement-Based Composite Transport Properties. *MRS Online Proceedings Library*, 245:265-270. https://doi.org/10.1557/PROC-245-265
[28] Gallé C (2001) Effect of Drying on Cement-Based Materials Pore Structure as Identified by Mercury Intrusion Porosimetry: A Comparative Study Between Oven-, Vacuum-, and Freeze-Drying. *Cement and Concrete Research*, 31(10):1467-1477. https://doi.org/10.1016/S0008-8846(01)00594-4

Appendix A. List of Symbols, Abbreviations, and Acronyms

A.1. Symbols

A
Cross-sectional area

b
Klinkenburg correction factor

k_A
Apparent permeability

k_0
Intrinsic permeability

L
Specimen thickness

L_{fm}
Reference length of soap bubble flow meter

p
Inlet pressure

p_a
atmospheric pressure

Q
Volumetric flow rate

$Q_{calculated}$
Q-value calculated from experimental data

$Q_{critical}$
Q-value obtained from Studentized Range Q table

S_{fm}
Cross-sectional area of soap bubble flow meter

t_I
Initial time of soap bubble flow meter reading

t_F
Final time of soap bubble flow meter reading

w/cm
Ratio of water to cementitious materials

α

significance level for statistical testing

$\alpha_{calculated}$

significance value calculated using experimental data

$\alpha_{corrected}$

corrected significance value using Bonferroni correction method

Δk_A

Difference in measured k_A values

μ
dynamic viscosity of gas at room temperature

A.2. Acronyms/Abbreviations

Cembureau
European Cement Association

ITZ
Interfacial transition zone

NSD
Not significantly different

RILEM
International Union of Laboratories and Experts in Construction Materials, Systems, and Structures

SD
Significantly different

SEM
Scanning electron microscope

Stdev
Standard deviation

A.3. General Chemistry Notation

$Fe_{1-x}S$
Pyrrhotite; x varies from 0 to 0.125

$Fe_{10}O_{14}(OH)_2$
Ferrihydrite

FeO(OH)
Goethite

SO_4^{2-}
Sulfate

A.4. Cement Chemistry Notation

A
Al_2O_3; corundum

C
CaO; quicklime

$\overline{C}$
CO_3; carbonate

H
H_2O; water

S
SiO_2; quartz

$\overline{S}$
SO_3; sulfur trioxide

C_3A
$3CaO \cdot Al_2O_3$; Tricalcium aluminate

$C_4A\overline{S}H_{12}$
$Ca_4Al_2O_6(SO_4) \cdot 14H_2O$; Calcium aluminate monosulfate hydrate

$C\overline{S}H_2$
$CaSO_4 \cdot 2H_2O$; Gypsum

$C_6A\overline{S}_3H_{32}$
$Ca_6Al_2(SO_4)_3(OH)_{12} \cdot 26H_2O$; Ettringite

$C_3S\overline{C}\text{-}\overline{S}\text{-}H_{15}$
$Ca_3Si(CO_3)(SO_4)(OH)_6 \cdot 12H_2O$; Thaumasite

CSH
$3CaO \cdot 2SiO_2 \cdot 3H_2O$; Calcium silicate hydrate